https://doi.org/10.5194/egusphere-2025-5228
Preprint. Discussion started: 25 November 2025

Culvert Blockages in 2D-Hydrodynamic Flood Modeling: Quantifying the Impact on Flood Dynamics and Designing Mitigation Strategies

Leon Frederik De Vos[1], Karan Mahajan[1], Daniel Caviedes-Voullième[2], and Nils Rüther[1]

[1]Chair of Hydraulic Engineering, Technical University of Munich, Munich, 80333, Germany
[2]Jülich Supercomputing Centre & Institute for Bio- and Geosciences, Forschungszentrum Jülich, Jülich, 52428, Germany

Correspondence: Leon Frederik De Vos (frederik.de-vos@tum.de)

Abstract.

Culverts play a critical role in conveying surface runoff during flash flood events, yet their failure due to blockages can significantly alter flood dynamics, particularly in small, topographically complex catchments. Despite this, culvert blockages are often neglected in flood modeling. To address such gap, this study presents a comprehensive analysis of culvert blockages using the open-source hydrodynamic model TELEMAC-2D, applied to a flash-flood-prone catchment in central Germany. First, the study assesses recent flood events and evaluates the completeness and accuracy of official culvert datasets, identifying missing culverts. A dynamic culvert blockage module is then implemented, simulating varying degrees and timings of blockage based on water level thresholds at culvert inlets. Through a series of flood scenarios, the study identifies culverts whose blockage has a major impact on flood hydrographs and inundation extents. Results highlight the importance of accurate culvert representation and demonstrate how scenario-based modeling of blockages can support the identification of critical infrastructure. This enables the development of targeted mitigation strategies, such as prioritized maintenance or emergency protection, ultimately reducing flood risks. The findings underscore the need to integrate culvert blockages into flash flood modelling and risk assessments and support future research into blockage formation mechanisms and improved field data acquisition.

1 Introduction

Floods have caused numerous catastrophic events in recent years, with increasing frequency and severity linked to climate change. Globally, rainfall extremes have reached record levels (Robinson et al., 2021), and projections suggest that these events will pose even greater risks in the future (Caretta et al., 2022). Especially short-duration, high-intensity rainfall events, often resulting in flash floods, are becoming more common and present specific challenges to flood modeling and hazard mitigation (Borga et al., 2014).

Flash floods occur globally (Gaume et al., 2009; Archer et al., 2019; Reinert et al., 2025; Okamoto et al., 2019), typically in small catchments with short response times (Lo´czy et al., 2012; Collier, 2007; Georgakakos, 1987; Voit and Heistermann, 2024). Due to the high rainfall intensity, water cannot be sufficiently infiltrated by the soil, resulting in rapid surface runoff. This runoff concentrates along topographic flow paths and is transported to lower elevations. When runoff exceeds local conveyance

https://doi.org/10.5194/egusphere-2025-5228
Preprint. Discussion started: 25 November 2025

capacity, minor watercourses or urban flowpaths can transform into powerful torrents with high flow velocities (Borga et al., 2008), capable of entraining debris such as sediment, vegetation, and floating objects (Bayón et al., 2024; Erpicum et al., 2024; Valero et al., 2024). This debris can significantly increase the hazard potential, particularly in urban environments where vulnerable infrastructure and people are concentrated.

To simulate such complex dynamics, hydrodynamic models must represent small-scale physical processes and flow-infrastructure interactions accurately. Recent advancements allow for direct rainfall input for hydrodynamic simulations using the rain-on-grid method. This enables the model to take spatially distributed precipitation as input and compute runoff at each element using empirical and physics-based methods (Ligier, 2016; De Vos et al., 2024) , such as the SCS-CN method (U.S. Department of Agriculture, Soil Conservation Service, 1972), or the Green-Ampt infiltration model (Green and Ampt, 1911).

In urban and peri-urban environments, accurate modeling of flash floods also requires fine spatial resolution to capture the onset of the flash flood along narrow topographic features (Caviedes-Voullième et al., 2012) and interactions with buildings and infrastructure (Schubert and Sanders, 2012) such as roads, and particularly culverts. Studies have shown that explicit modeling of these components significantly improves simulation accuracy (Ah-Woane et al., 2025; Pizzileo et al., 2024; Bowling and Lettenmaier, 1997).

However, calibration of flash flood models remains challenging due to limited data availability. Flash floods often occur in small, ungauged catchments, and their short duration makes in-situ monitoring difficult (Borga et al., 2008). As a result, photographic documentation, reports from local residents, and citizen science initiatives are often the only sources of validation data (Khosh Bin Gomash et al., 2025; Rohmat et al., 2022). Arguably, flash flood models are the only available source to provide high-resolution spatial-temporal outputs of water depths and velocities, which are crucial for flood forecasting, hazard assessment, and evacuation planning (Apel et al., 2008; Khosh Bin Ghomash et al., 2024; Li et al., 2025).

Furthermore, hydrodynamic flood models are used to evaluate the effectiveness of flood mitigation measures, both by permanent structural measures, such as retention basins, or temporal operational measures, such as temporary flood protection walls or maintenance of critical hydraulic infrastructure.

Hydraulic infrastructure can have large impacts on floods. Bridges can cause backwater effects, if logjams of floating debris are formed upstream of the bridge (Burghardt et al., 2025; Okamoto et al., 2019). However, these logjams at bridges usually show larger impacts at larger bridges, which are present at large rivers and therefore not directly an issue for flash floods at smaller streams. Culverts ensure stream connectivity across infrastructure such as roads or railway embankments, often turning into critical bottlenecks during flood events. During flash floods, floating or sediment-laden debris can obstruct culvert inlets, reducing discharge capacity and leading to upstream ponding, elevated flood levels, and increased flow velocities at outlets. In extreme cases, this may result in embankment failure due to scour or seepage (Rigby et al., 2002). Even without structural failure, blocked culverts substantially affect local flood behavior and must be accounted for in realistic modeling scenarios.

Therefore, blocked culverts have been studied in laboratory experiments, and equations to incorporate the reduced discharge capacity of blocked culverts have been developed (Weeks et al., 2013; Miranzadeh et al., 2023; Sellevold et al., 2024; Rigby and Barthelmess, 2011). However, mainstream hydrodynamic models rarely incorporate dynamic culvert blockage representations.

https://doi.org/10.5194/egusphere-2025-5228
Preprint. Discussion started: 25 November 2025

For instance, Ollett et al. (Ollett et al., 2017) present their implementation of a static blockage module in TUFLOW, and refer to future studies for a dynamic culvert blockage.

The lack of dynamic culvert blockage models can be linked to at least two challenges: First, culvert blockage mechanisms are highly site-specific and depend on local topography, available debris load and type, and culvert design. Second, the timing and degree of blockage cannot be predicted (Rigby and Barthelmess, 2011) and must be assumed or parameterized using probabilistic or threshold-based approaches (Ball et al., 2019). The Australian Rainfall and Runoff Guidelines, therefore, recommend using unblocked culverts as a reference scenario, and simulating blockage scenarios across a range of parameters to assess their potential impact. For an in-depth analysis into the types, mechanisms and probabilities of culvert blockages the present study refers to chapter 6 of the Australian Rainfall and Runoff Guideline for Flood Estimation (Ball et al., 2019).

While some studies have started to address the research gap of modeling blocked culverts within a catchment, few have examined both local and catchment-scale effects. Ah-Woane et al. (2025) modeled dynamic culvert blockages in the Brague catchment in southern France. Blockage onset was triggered at maximum culvert inflow or when bankfull conditions were reached. They observed limited impacts on downstream hydrographs, but noted that local flow dynamics were affected. However, the specific configuration of their case study, where all culverts passed under the same highway, allowed floodwaters to rejoin the downstream system, minimizing the blockage's overall effect. (Rigby and Barthelmess, 2011) simulated the effects of a single blocked culvert for multiple blockage degrees and timing points, but did not investigate the effects on a catchment with multiple culverts. Their study also identified the need for more research on the impacts of culvert blockages.

To address the current research gap, the present study provides a comprehensive analysis of culvert blockages in flash flood modeling, evaluating their impact both on a local and a catchment scale. It applies the open-source model TELEMAC-2D (EDF, 2022) to the flash-flood-prone catchment of Reichenberger Bach in central Germany. TELEMAC-2D is well-suited for this purpose due to its support for unstructured meshes, in turn permitting fine local spatial resolution, and its parallel processing capabilities, allowing it to accurately simulate complex flow conditions along fine topographic flow paths or urban areas.

First, this study analyzes recent flood events in the catchment, followed by a detailed description of the model setup, infrastructure representation, and culvert integration. As a first result, this study stresses the importance of assessing official culvert datasets and identifying missing or inaccurately represented culverts, which are often absent from infrastructure records. The proper representation of culverts is essential for reliably simulating flood pathways, connectivity, and ponding effects in small catchments.

A dynamic blockage module is then implemented in TELEMAC-2D and applied for multiple flood scenarios, triggering different partial blockages based on water level thresholds at culvert inlets.

By analyzing hydrographs and inundation extents across the different blockage scenarios, the study identifies critical culverts — those whose blockage disproportionately affects flood dynamics. This facilitates the development of targeted mitigation scenarios, such as designating certain culverts for maintenance or protection during early warning phases.

https://doi.org/10.5194/egusphere-2025-5228
Preprint. Discussion started: 25 November 2025

The study concludes by demonstrating how blocking or safeguarding specific culverts changes flood outcomes, potentially reducing flood hazards and associated damages. This integrated modeling approach provides valuable insights for risk-informed planning, emergency preparedness, and infrastructure maintenance.

2 Materials and Methods

2.1 Study Area

The investigated study area is the ungauged catchment of the Reichenberger Bach with an area of approx. 33 km^2 (see red outline in Figure 1). The Reichenberger Bach merges with the Fuchsstädter Bach shortly downstream of the study area outlet and flows into the River Main south of Würzburg in the Northeast of Bavaria, Germany. The study area has high gradients with the topography ranging from 191 m.a.s.l. at the outlet to 374 m.a.s.l. at the northwest watershed boundary. Two distinct major streams can be identified in the catchment. The first stream is the Reichenberger Bach, which flows from south to north, mainly surrounded by agricultural fields and passing through some villages. The second stream (Guttenberger Bach) flows from the northwest watershed boundary towards the municipality of Reichenberg, where it merges into the Reichenberger Bach within an underground duct. The Guttenberger Bach mainly flows through forested land. In general, both the Reichenberger Bach as well as the Guttenberger Bach are mainly flowing beneath the municipality of Reichenberg.

Numerous culverts are usually located in catchments like the one in this study (see Figure 1). The data provided by the environmental administration agency in Bavaria, Germany (LfU), included 22 culverts. During the first model runs, it became evident that culverts were missing in the provided data, as inundation areas were forming at elevated roads and railway tracks. An additional seven culverts were identified at some of these inundation areas, and surveyed, during a site inspection. These 7 culverts must be represented in the model to enhance the quality of the model results, as they impact the flood dynamics. However, it is unlikely that all culverts within the study area were identified; therefore, some minor culverts are most likely undetected.

The culverts in the study area can be separated into two groups:

1. In-stream culverts: Culverts that are directly along the major streams. These culverts were all represented in the data set from the authorities.

2. Towards-stream culverts: Culverts that connect minor streams with the major streams. Here, 7 additional culverts were found. Without these culverts, the sub-catchments upstream of the culverts are disconnected from the overall flood.

2.2 Precipitation Scenarios

Even though the Reichenberger Bach lies in a comparatively dry region with a mean annual precipitation of 712 mm (Bayerisches Landesamt für Umwelt, 2021), the catchment area of the Reichenberger Bach has experienced several minor flash flood events caused by heavy precipitation in recent years:

https://doi.org/10.5194/egusphere-2025-5228
Preprint. Discussion started: 25 November 2025

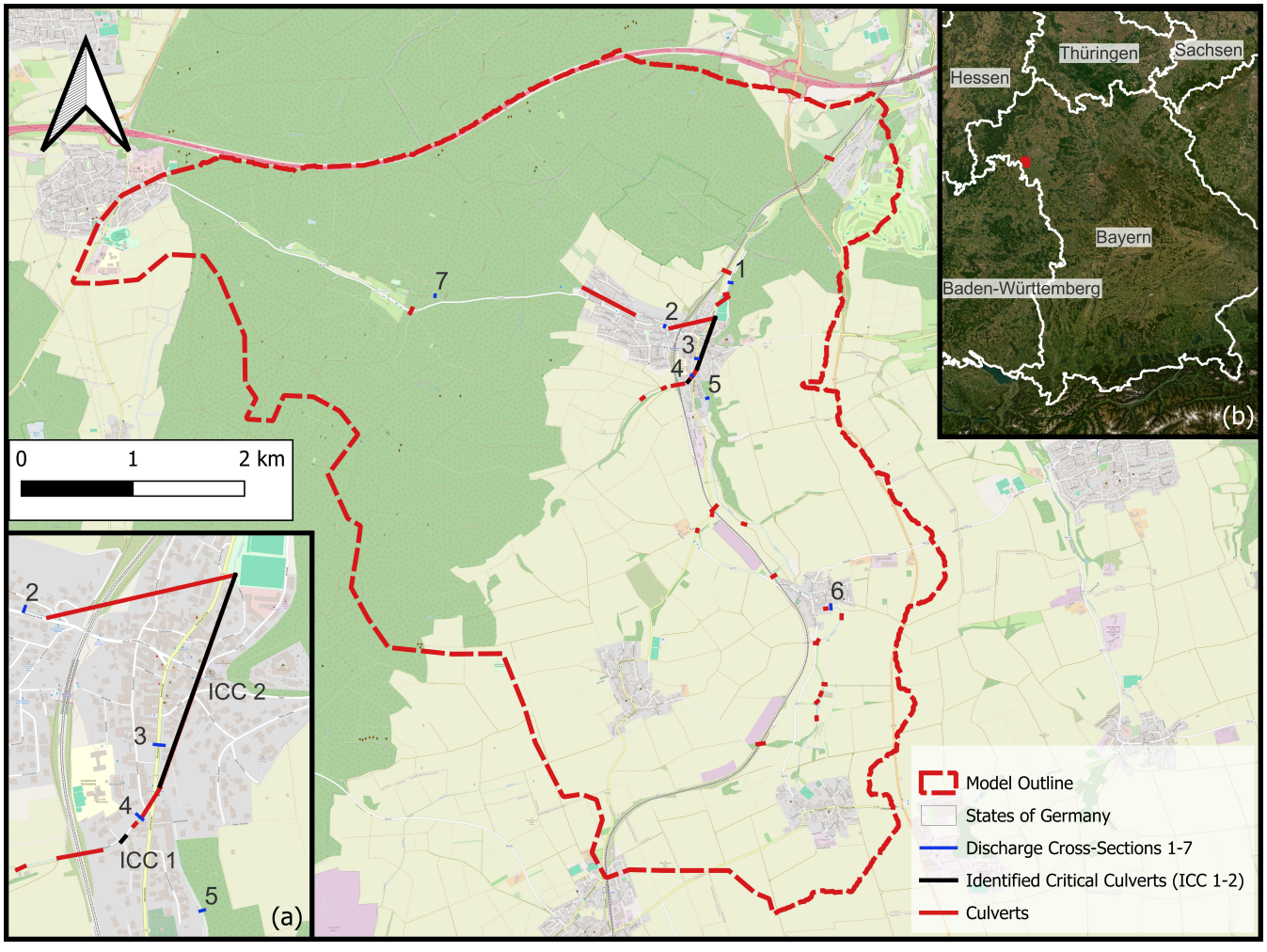

Figure 1. The catchment of the study area. The dashed red line shows the catchment boundary. Solid red lines depict the complete culvert data set, with the black lines being the critical culverts identified in this study. Blue lines are the numbered cross-sections used for hydrograph analysis in the catchment. Map inset (a): a detailed view of the location of the critical culverts in Reichenberg. Map inset (b): The position of the catchment in the north west of Bavaria, a Federal State in Germany. Basemaps from © OpenStreetMap contributors 2025, distributed under the Open Data Commons Open Database License (ODbL) v1.0, and Esri (2025).

1. 28th of June 2021: 30 mm of precipitation in 3 hours (rainfall event with a three year return period, HN3), locally up to 37 mm in 3 hours (HN10)
2. 9th of July 2021: 60 mm in 13 hours (HN20)
3. 15th of July 2021: 25 mm in 2 hours (HN3), but locally up to 43 mm in 2 hours (HN30)
4. 3rd of August 2024: 29 mm in 3 hours (HN3), but locally up to 43 mm in 3 hours (HN20)

https://doi.org/10.5194/egusphere-2025-5228
Preprint. Discussion started: 25 November 2025

Events 1–3 were obtained from the hourly RADKLIM data set (Winterrath et al., 2018b), whereas the fourth event was obtained from the recent hourly RADOLAN data set (DWD Climate Data Center (CDC), 2025; Bartels et al., 2004). The return periods were compared to the KOSTRA 2020 data set (Junghänel et al., 2022). All events caused multiple fire department operations due to flooded streets and basements (Feuerwehr Reichenberg, 2021b, a, 2024).

To cover a broad range of precipitation scenarios, return periods from 5 to 100 years are modelled (see Table 1 for the temporal distributions). The precipitation intensities are taken from the KOSTRA 2020 data set (Junghänel et al., 2022) and temporally distributed using the Euler II distribution (Deutsche Vereinigung für Wasserwirtschaft, Abwasser und Abfall, 2006), which arranges the higher intensities in ascending order over the first third of the scenario and the lower intensities in descending order over the rest of the scenario. The precipitation is assumed to be spatially uniform. After conducting simulations with different precipitation durations, the highest peak discharges were present for precipitation durations of 6 hours. Therefore, the overall duration of the investigated precipitation scenarios in this study was set to 6 hours. The precipitation serves as an input for the SCS-CN model (U.S. Department of Agriculture, Soil Conservation Service, 1972) that calculates the surface runoff. The total duration of the modelled floods is 10 hours to ensure that the flood peak has propagated throughout the catchment.

Table 1. Precipitation values (incremental and cumulative in mm) for various return periods and time intervals.

Time	HN5	HN10	HN20	HN30	HN50	HN100
0 min	0.0 (0.0)	0.0 (0.0)	0.0 (0.0)	0.0 (0.0)	0.0 (0.0)	0.0 (0.0)
30 min	2.0 (2.0)	2.3 (2.3)	2.7 (2.7)	2.9 (2.9)	3.3 (3.3)	3.7 (3.7)
1 h	2.7 (4.7)	3.2 (5.5)	3.6 (6.3)	3.9 (6.8)	4.3 (7.6)	4.9 (8.6)
1 h 15 min	1.8 (6.5)	2.1 (7.6)	2.4 (8.7)	2.7 (9.5)	2.9 (10.5)	3.3 (11.9)
1 h 30 min	2.4 (8.9)	2.8 (10.4)	3.3 (12.0)	3.5 (13.0)	3.9 (14.4)	4.4 (16.3)
1 h 40 min	2.3 (11.2)	2.6 (13.0)	3.0 (15.0)	3.3 (16.3)	3.7 (18.1)	4.2 (20.5)
1 h 45 min	1.5 (12.7)	1.9 (14.9)	2.1 (17.1)	2.3 (18.6)	2.5 (20.6)	2.9 (23.4)
1 h 50 min	2.1 (14.8)	2.5 (17.4)	2.9 (20.0)	3.2 (21.8)	3.5 (24.1)	4.0 (27.4)
1 h 55 min	3.6 (18.4)	4.1 (21.5)	4.8 (24.8)	5.1 (26.9)	5.7 (29.8)	6.4 (33.8)
2 h	10.6 (29.0)	12.5 (34.0)	14.4 (39.2)	15.7 (42.6)	17.3 (47.1)	19.7 (53.5)
3 h	3.0 (32.0)	3.6 (37.6)	4.2 (43.4)	4.5 (47.1)	5.0 (52.1)	5.6 (59.1)
4 h	2.3 (34.3)	2.7 (40.3)	3.1 (46.5)	3.4 (50.5)	3.7 (55.8)	4.3 (63.4)
6 h	3.6 (37.9)	4.2 (44.5)	4.8 (51.3)	5.2 (55.7)	5.8 (61.6)	6.5 (69.9)
Total Prec.	**37.9**	**44.5**	**51.3**	**55.7**	**61.6**	**69.9**

2.3 Mesh Generation and Parameters

The mesher triangle (Shewchuk, 1996) is used to generate a Delaunay triangulation. To precisely incorporate the topographical stream paths, a watershed delineation is conducted and stream paths with a Strahler Order of 7 or lower are included as breaklines with a resolution of 0.5-0.7 m. Additionally, areas with measured channel geometries were refined with a resolution

https://doi.org/10.5194/egusphere-2025-5228
Preprint. Discussion started: 25 November 2025

of approximately 0.7 m. These areas cover the Reichenberger Bach and some sections of tributaries upstream of their confluence with the Reichenberger Bach. The stream paths, together with the refined areas of channel geometries, represent all the major flow paths in the hydrodynamic model in detail. Buildings close to the channels are represented as holes in the mesh and their edges are resampled with a resolution of 1-2m. Buildings farther away from the channels and located higher above the channels are neglected as the flood inundation from the overtopped channels cannot extend to those buildings, and therefore, they do not influence hydrodynamic processes. Their influence on the rainfall-runoff process is deemed insignificant due to the low area percentage covered by buildings in the rural surroundings. Outside of the refined channels, stream paths, and buildings, the mesh coarsens to a resolution of 15 m. In total, the mesh has 1,168,050 nodes and 2,318,072 elements. The topography of the model is generated in two steps. First, the digital elevation model, which is also used for watershed delineation, is interpolated on the mesh. Then, the bathymetry within the refined channel areas is interpolated from an existing flood model provided by the authorities, where the bathymetry was based on measured channel geometries. The digital elevation model and the measured channel geometries were both provided by LfU Bayern. Furthermore, the LfU Bayern provided land use data, which were taken to map roughness values based on administrational guidelines (LUBW, 2020) and generate the CN values for the applied SCS-CN rainfall-runoff method (U.S. Department of Agriculture, Soil Conservation Service, 1972).

The 2D-hydrodynamic module TELEMAC-2D from the open-source software TELEMAC (EDF, 2022) is applied to solve the shallow water equations and simulate the flood scenarios using a timestep of 0.5 s for the semi-implicit solver in the finite-element method. The initial conditions assume a completely dry state, since most of the channels in the catchments only carry little to no water without a preceding rain event. Since the catchment is topographically bounded, there are no discharge inlets, and all water comes from the rain input applying the implemented SCS-CN method for rainfall-runoff modelling. The catchment outlet is modelled as a free outlet boundary condition.

2.4 Model Validation

In general, data sets for flooding in catchments as in this study are scarce due to the short duration and local focus of the rain events (Khosh Bin Gomash et al., 2025). Since the catchment is also ungauged, the model cannot be calibrated using the outlet hydrograph. The best available data set for model validation are photographs from the flood event on 15th of July 2021. These photographs were used to generate a water mask during a field campaign in the catchment (Figure 2). However, this water mask does not provide any temporal information and cannot be interpreted as a maximum inundation extent but serves as a snapshot in time or a minimum inundation extent if the photograph does not have any timestamp. Additionally, there is no indication about areas not covered by any photograph. These areas might have been inundated or not and no validation of these areas in the model is possible.

The validation event on the 15th of July 2021 caused, in total, 29 calls to the fire department, more than the 18 calls for the directly preceding event on the 9th of July 2021 ((Feuerwehr Reichenberg, 2021c)). As the rainfall amount and return period of the event on the 9th of July was higher (60 mm in 13 hours, HN20, see section 2.2), the increased damage by the flood cannot stem from the precipitation. Therefore, we assume that the soil in the catchment on the 15th of July was still saturated from the flood event on the 9th of July. To take this into account, the antecedent moisture in the SCS-CN method

https://doi.org/10.5194/egusphere-2025-5228
Preprint. Discussion started: 25 November 2025

Figure 2. Generating a water mask from a recent flood event using photographs. Left: Sampling water extension points from the water mask using an Emlid GPS-system. Right: Photograph from the flood event on 15th of July 2021.

is set to wet conditions, which effectively increases the CN values (Hawkins, 1978) and, therefore, the runoff. To minimize the uncertainty of the precipitation input, a spatially distributed precipitation is applied for the validation event. For this, the 5-minute RADOLAN-Y precipitation data with a pixel size of approximately 1x1 km (Winterrath et al., 2018a) is interpolated onto the model and used as input for the SCS-CN method.

Figure 3 compares the water extension from the simulation of the validation event with the measured water extension points at two distinct locations. At the location on the left, some water extension points are not fully reached in the simulation. On the right, the simulated water extension has a good fit with the measured water extension. Since the data retrieved from the photographs already incorporate uncertainties and are only limited to specific locations, no local model adaptations with respect to friction coefficients or runoff coefficients were conducted.

2.5 Culvert Modeling in TELEMAC-2D

Culverts are a hydraulic infrastructure that ensures stream connectivity through or beneath topographic barriers. These topographic barriers are mainly roads or railway tracks. Still, sometimes a longer stretch of a stream can be moved entirely underground to cope with spatial constraints in settled areas, thereby bypassing whole villages. Even though the geometry and setup of a culvert itself appear relatively simple, culverts pose considerable challenges in hydraulic modeling (Ball et al., 2019). This is due to the complex flow behavior of culverts, which can be classified into six different types (Bodhaine, 1968).

Each flow type is defined by the flow in the barrel (full or partly full), culvert slope, and specific ranges in the ratios of the upstream and downstream water depths to the culvert diameter. The flow types can be further grouped into inlet (flow types 1 and 5) and outlet control (flow types 2, 3, 4, and 6). Under inlet control, the flow is partly full in the barrel and supercritical

https://doi.org/10.5194/egusphere-2025-5228
Preprint. Discussion started: 25 November 2025

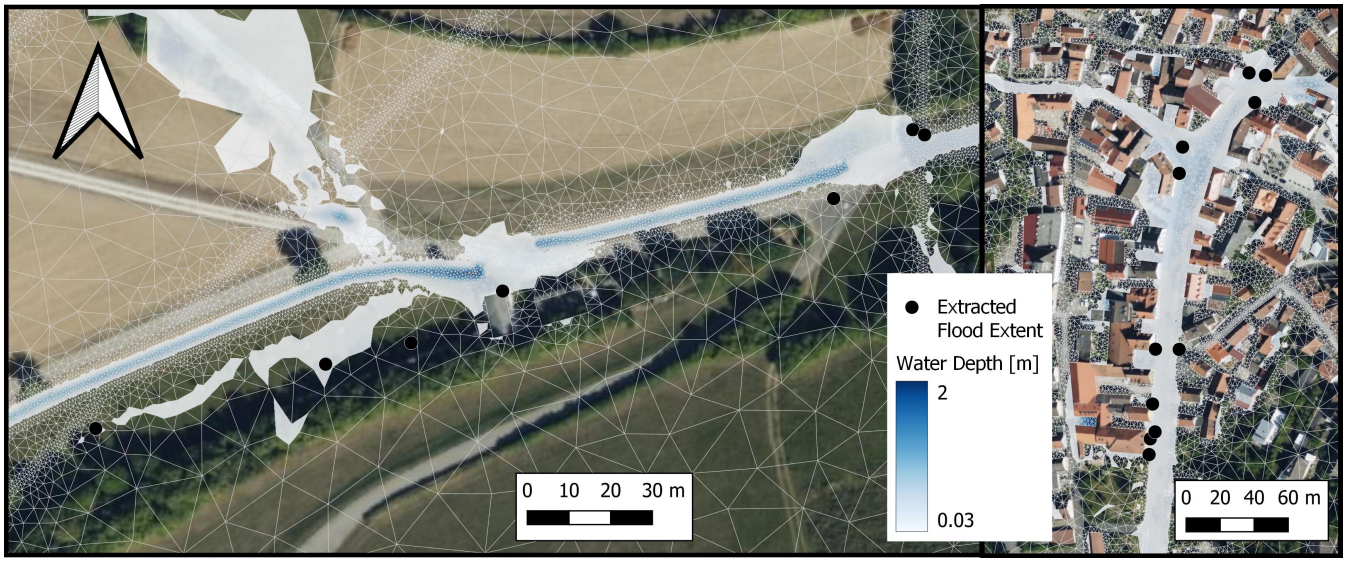

Figure 3. Points of measured flood extent and simulated water extension for the validation event. Basemaps: Bing Maps © Microsoft Corporation and its data providers.

before the culvert outlet. Therefore, the flow only depends on the water depth and geometry at the inlet. Otherwise, the flow is under outlet control and depends also on the water depth and geometry at the outlet. An in-depth description of the hydraulics of culverts is given in Bodhaine (1968).

TELEMAC-2D models culverts as a 1D sink and source link from an upstream node representing the culvert inlet to a downstream node (outlet). The discharge calculation follows the equations from Bodhaine (1968), yet flow type 1 is not implemented due to its rare occurrence (Smolders et al., 2016). First, the discharge through the culvert Q_{Cul} is calculated based on the flow type. Then, it is checked whether the upstream node holds enough available water to fulfill the calculated culvert discharge. The available water per time step at the node is calculated using the water depth h at the upstream node, the element area A_{elem} of the upstream node, and the time step dt. This sets an upper limit for the maximum discharge Q_{max} through the culvert in the model:

$$Q_{\text{max}} = \frac{h \cdot A_{\text{elem}}}{dt} \cdot k \tag{1}$$

Factor k is set to 0.9 by default in TELEMAC-2D to ensure the element does not fully dry. In practice, culverts usually span across most of the stream to avoid backwater rising for small discharges. To capture the 2D flow dynamics of the stream in the numerical model, multiple nodes must be laid laterally across the stream, yet only one single node contributes to the discharge through the culvert. Therefore, the calculated discharge through the culvert Q_{Cul} might be larger than the limit for the maximum discharge Q_{max}, and not enough water can be transported through the culvert in the model. As indicated in (1),

https://doi.org/10.5194/egusphere-2025-5228
Preprint. Discussion started: 25 November 2025

this limitation could be addressed by reducing the time step of the model. However, this would significantly increase the model runtime and is therefore not considered practical.

Consequently, this study extends the existing culvert implementation in TELEMAC-2D. First, the factor k is reduced to 0.5 to limit the maximum volume reduction at the culvert inlet node. Then, if the calculated discharge through the culvert Q_{Cul} exceeds the maximum discharge Q_{max}, the residual discharge is distributed onto neighboring nodes. This improves numerical stability and allows the full theoretical discharge to be transported to the outlet. Similar culvert-handling methods are not only presented in Fernández-Pato et al. (2020), but might also be introduced in future TELEMAC-2D releases (Smolders and Bourbain, 2024).

2.6 Blockage Methods and Scenarios

Since the study area lies in forested and agricultural lands with high gradients, its culverts are prone to logjams (Ball et al., 2019; Rigby et al., 2002), as also demonstrated in photographs from the site inspection and recent flood events (see Figure 4, middle and right). Culvert blockages are usually modelled either using the area reduction method (ARM), which reduces the culvert diameter or height, or the energy loss method (ELM), which increases the energy loss coefficient at the inlet of the culvert k_e (Weeks et al., 2013). The ARM seems to be suitable for sedimentation blockages since the sediment fills up the culvert from bottom to top, and therefore, the bottom elevation of the culvert can still be defined. However, the sedimentation of the study area's culverts is minimal and, therefore, can be neglected (see Figure 4, left).

For logjam blockages, an entangled body of wood logs and branches is captured in front of the inlet of the culvert (see Figure 4, middle and right). Since the effective loss of the inlet area cannot be strictly accounted for in the bottom or top part of the culvert, this study applies the ELM (energy loss method). The ELM is only applicable for outlet control conditions in culverts (Ollett et al., 2017), and not for inlet control conditions. However, during a flood event, culverts are mainly in outlet conditions, as can be deduced by the definition of the control conditions and flow types through culverts (Bodhaine, 1968; Smolders et al., 2016).

The ELM is based on an increase in the inlet loss coefficient of the culvert based on the blockage ratio BR, defined as the ratio of obstructed culvert area to the overall culvert area without any logjam. Since logjam bodies are complex and heterogeneous in all three dimensions, they are often modeled as porous bodies, impeding the estimation of BR with absolute certainty (Iqbal and Riaz, 2024). Therefore, this study investigates blockage scenarios with $BR = 0.2$, 0.5, and 0.8 to account for different degrees of blockage. Based on these blockage ratios, the corresponding adapted energy loss coefficient at the inlet k_e' can be calculated according to Ollett et al. (2017); Weeks et al. (2013) as:

$$k_e' = \left(\frac{1 + \sqrt{k_e}}{1 - BR} - 1 \right)^2 \tag{2}$$

where the initial energy loss coefficient at the inlet without blockage, k_e, is set to 0.5 in this study. For $BR = 0.2$, 0.5, and 0.8, the adapted energy loss coefficient at the inlet k_e' increases to 1.3, 5.8, and 56.8, respectively.

https://doi.org/10.5194/egusphere-2025-5228
Preprint. Discussion started: 25 November 2025

Figure 4. left: inspection of an unsurveyed culvert with slight sedimentation, middle: extreme logjam in front of an unsurveyed culvert (see black circle for culvert location), right: blocked culvert during the flood event at 9th of July, 2021 (Feuerwehr Reichenberg (2021b), https://ff-reichenberg.de/einsatzberichte/1752-hochwasser-strasse-ueberflutet/)

Furthermore, the scenarios differ in the timing of the blockage. Blockages are based on the trigger ratio TR, which is defined as the ratio of the water depth at the culvert inlet H_i and the inlet height or diameter of the culvert D:

$$TR = \frac{H_i}{D} \tag{3}$$

TR is predefined for each scenario, ranging from $TR = 0$ (initial blockage at all culverts) to $TR = 1.5$ (blockage when water depth at inlet is 1.5 times the inlet height). Once the blockage of a culvert is triggered, it cannot be unblocked again, even if TR falls below the defined trigger threshold after the flood peak. The ELM was implemented into the culvert module of TELEMAC-2D for this study.

The scenarios investigated in this study trigger the blockages for $TR = 0.8$, 1.0, 1.2, and 1.5. Table 2 shows the investigated combinations of scenarios with BR and TR. To reduce computational time, not all possible scenario combinations have been simulated. Each blockage scenario was modeled for rainfall return periods of HN5, HN10, HN20, HN30, HN50, and HN100 (see Section 2.2). The reference scenarios incorporate no blockages.

Different TRs cause a different amount of culverts to be blocked during the simulation. A lower TR will increase the number of culverts for which blockage is triggered. This allowed to assess the impact of additionally triggered culverts. Therefore, in addition to the BR and TR scenarios listed in Table 2, some additional scenarios accounting for blockage mitigation measures

https://doi.org/10.5194/egusphere-2025-5228
Preprint. Discussion started: 25 November 2025

Table 2. Investigated blockage scenarios for different blockage ratios (BR) and trigger ratios (TR).

BR \TR	0 (initial)	0.8	1.0	1.2	1.5
0.2	–	X	–	–	X
0.5	–	X	–	–	X
0.8	X	X	X	X	X

by first responders have been modelled. These scenarios ensure that some culverts cannot be blocked during the flood event ($TR = \infty$), which in practice corresponds to the fire department or other first responders actively removing floating debris and small logjam bodies from the culvert inlets. These scenarios are based on the analysis of the scenarios in Table 2 and will be explained in more detail in section 3.5.

3 Results & Discussion

3.1 Influence of Missing Culverts in Data Set from Authorities

An initial model comparison is conducted to highlight the significance of incorporating all culverts within the study area. To this end, simulations were conducted for all rainfall return periods using two configurations: one that includes only the culverts listed by the authorities, and another that incorporates all identified culverts.

Table 3 lists the peak discharges at the catchment outlet for both configurations across all return periods. Although the absolute differences in peak discharge are relatively small, the relative differences range from 4.9% to up to 8.6%, underscoring the potential impact of an incomplete culvert data set on flood modeling outcomes.

Table 3. Peak discharge $Q_{\max}$ [m^3/s] for different rainfall return periods without any blockages, once incorporating all located culverts and once only the culverts from the authorities' data set. Additionally, the relative difference (Rel. Diff.) in peak discharge is listed.

Return Period	All culverts [m^3/s]	Authorities culverts only [m^3/s]	Rel. Diff. [%]
HN5	4.1	3.9	-5
HN10	7.4	6.8	-8
HN20	11.6	10.6	-9
HN30	14.8	13.7	-7
HN50	19.7	18.5	-6
HN100	28.7	26.9	-6

Since the additional culverts are all towards-stream culverts, it can indeed be expected that their inclusion leads to an increase in simulated discharge, as illustrated by the hydrographs in Figure 5. Notably, the increase in discharge coincides with the overall flood peak, suggesting that the response times of the contributing subcatchments align closely with the overall catchment response.

https://doi.org/10.5194/egusphere-2025-5228
Preprint. Discussion started: 25 November 2025

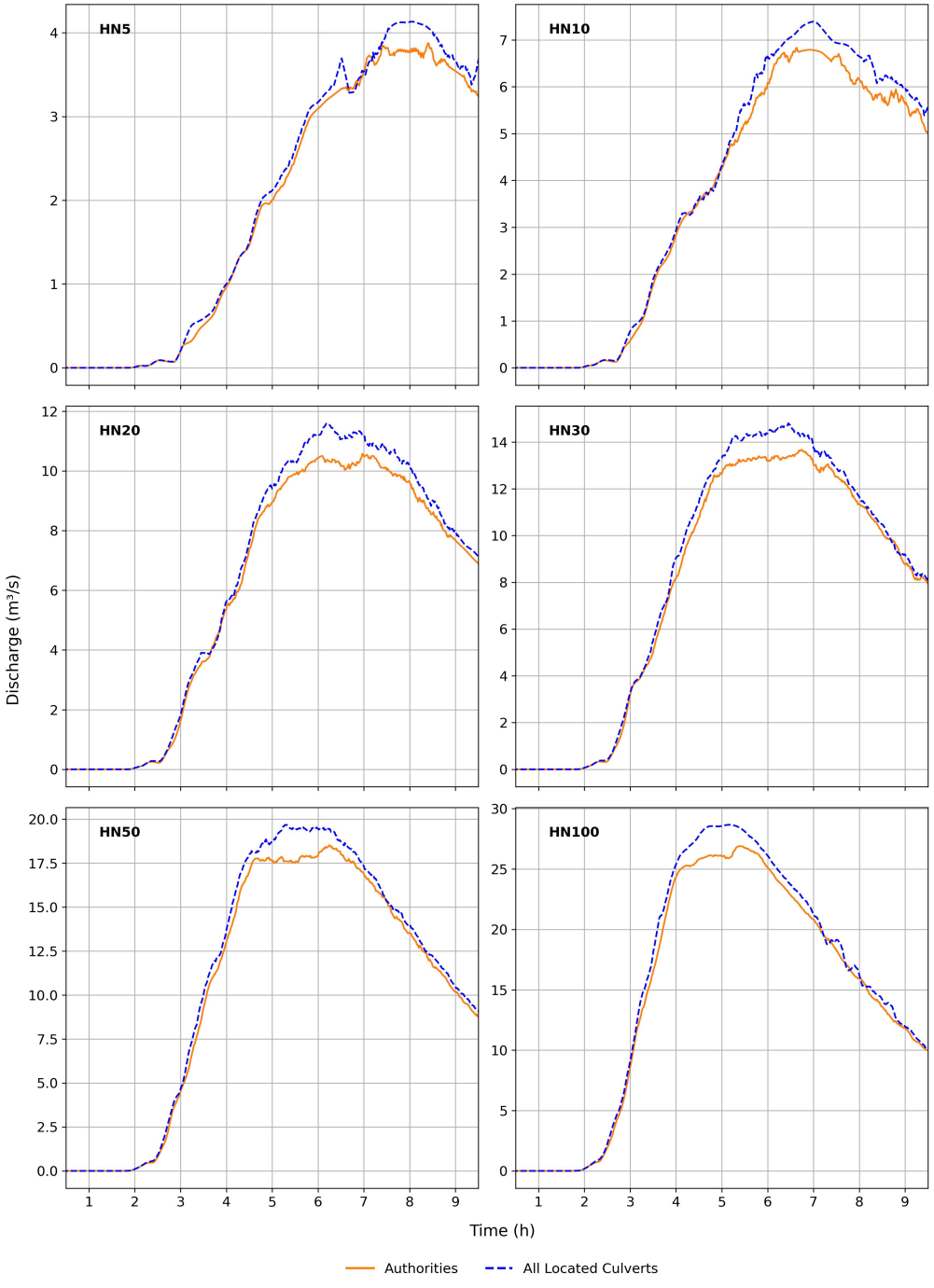

Figure 5. Outlet hydrographs for the different rainfall return periods, once incorporating all located culverts and once only the culverts from the authorities' data set

https://doi.org/10.5194/egusphere-2025-5228
Preprint. Discussion started: 25 November 2025

While this characteristic could be specific to the catchment investigated in this study and has not been proven to be generalizable to others, the findings underscore the importance of using a comprehensive culvert dataset. Omitting culverts in hydrodynamic models can cause parts of the catchment to become artificially disconnected from the flood dynamics, resulting in an underestimation of downstream discharge and flood extent. It could also, in turn, result in an overestimation of flood extent upstream of the missing culverts.

It is also important to acknowledge that some culverts within the study area may still be undiscovered, and hence unaccounted for. As a result, the simulated outlet hydrographs are likely to be still underestimated. However, since additional culverts were specifically identified in areas of pronounced inundation, it is less likely that the remaining unidentified culverts would substantially alter the peak discharge at the outlet.

3.2 Impact of Blockage Scenarios on Outlet Hydrograph

The impact of culvert blockages on hydrographs at the outlet of the study area is first assessed. A blocked culvert increases water levels upstream due to restricted flow, which can lead to expanded upstream inundation areas and temporary water retention. Consequently, blocked culverts are expected to reduce the discharge at the catchment outlet. However, the extent of discharge reduction depends on several factors:

1. Upstream topography: In steep terrain, the potential storage volume gained from increased water depth is limited compared to flat terrain, where broader inundation areas can develop.

2. Crest height of topographic obstacle: Culverts typically cut through embankments or artificial barriers such as roads, railways, dams or levees. The higher the crest elevation of such structures, the greater the upstream retention potential. Once overtopping occurs, the retention effect diminishes as water is redirected downstream via the overtopped path.

3. Blockage ratio BR: Higher blockage ratios correspond to more severe flow constrictions, leading to greater energy loss at the culvert inlet. This results in higher upstream water levels and, consequently, greater retention potential.

4. Timing of triggered blockage: The onset of a blockage has an immediate impact on upstream water levels. The timing is controlled by the trigger ratio (TR), where higher TR values delay the onset of blockage. Lower TR values may trigger blockage too early for a retention effect at the peak discharge, whereas higher TR values may not trigger blockage at all.

Table 4 presents the peak discharges for scenarios with varying trigger ratios TR and blockage ratio $BR = 0.8$ after triggered blockage across different return periods. The relative differences in peak discharge compared to the corresponding reference scenarios are also provided. For return periods greater than HN5, the observed reduction in peak discharge remains below 2%, indicating that the influence of culvert blockages is limited at the catchment outlet. These findings are consistent with those reported by Ah-Woane et al. (2025).

Figure 6 provides a detailed comparison of outlet hydrographs across all return periods by juxtaposing the reference scenario with blockage scenarios featuring different trigger ratios TR. For all return periods except HN5, the hydrographs exhibit only minor deviations between the reference and blockage scenarios. The most noticeable differences occur in the ascending limb

https://doi.org/10.5194/egusphere-2025-5228
Preprint. Discussion started: 25 November 2025

Table 4. Peak discharge (Max. Q) and relative difference (Rel. Diff.) for various trigger ratio (TR) scenarios.

Return Period	Reference (TR = ∞)	TR = 0		TR = 0.8		TR = 1.0		TR = 1.2		TR = 1.5	
	Max. Q [m^3/s]	Max. Q [m^3/s]	Rel. Diff. [%]	Max. Q [m^3/s]	Rel. Diff. [%]	Max. Q [m^3/s]	Rel. Diff. [%]	Max. Q [m^3/s]	Rel. Diff. [%]	Max. Q [m^3/s]	Rel. Diff. [%]
HN5	4.1	4.0	-2.4	4.0	-2.4	4.2	2.4	4.4	7.3	3.9	-4.9
HN10	7.4	7.3	-1.4	7.3	-1.4	7.3	-1.4	7.3	-1.4	7.4	0.0
HN20	11.6	11.5	-0.9	11.4	-1.7	11.4	-1.7	11.4	-1.7	11.4	-1.7
HN30	14.8	14.6	-1.4	14.7	-0.7	14.7	-0.7	14.5	-2.0	14.8	0.0
HN50	19.7	19.3	-2.0	19.6	-0.5	19.5	-1.0	19.8	0.5	19.6	-0.5
HN100	28.7	28.1	-2.1	28.5	-0.7	28.4	1.0	28.6	-0.3	28.5	-0.7

of the hydrographs, specifically within the discharge range of approximately $Q = 2m^3/s$ to $4m^3/s$. In this range, all blockage scenarios demonstrate a slight reduction in discharge relative to the reference. Although this effect is less visually prominent for higher return periods - primarily due to the scale of the y-axis - it remains present. The observed discharge reduction can be attributed to a single culvert blockage that increases the water depth upstream of the inlet, subsequently activating an adjacent floodplain and reducing downstream flow. Notably, the scenario with $TR = 1.5$ shows a delayed onset of this retention effect compared to scenarios with lower TR values, which is expected since blockage is only triggered once a higher water depth–to–culvert diameter ratio is reached.

Although these blockage-induced effects have limited influence on the peak discharge at the outlet, they suggest a potentially more substantial impact on flow dynamics within individual subcatchments. Consequently, hydrographs at selected cross-sections throughout the study area are analyzed in the following section to assess the localized effects of culvert blockages on flood behavior.

3.3 In-Depth Analysis of Hydrographs at Selected Cross-Sections

Hydrographs at seven cross-sections distributed throughout the catchment (see Figure 1) were analysed to assess the local impact of culvert blockages. Detailed hydrograph plots for each cross-section are provided in. A detailed figure for each cross-section can be found in Appendix A, Figures A1 through A7.

1. Cross-section 1 lies downstream of the municipality of Reichenberg, just below the piped sections of the Reichenberger Bach. The hydrographs closely resemble those at the catchment outlet, with minor differences visible in the peak discharges for the HN20 and HN30 scenarios, where the reference scenario shows slightly lower peaks.

2. Cross-section 2 is positioned at the end of the Guttenberger Bach, prior to its transition into an underground conduit and confluence with the Reichenberger Bach. For HN5 and HN10, the hydrographs exhibit negligible differences. For HN20, only the reference and $TR = 1.5$ scenarios show a delayed flood peak. For HN30, HN50, and HN100, the peak discharges are higher in the reference and $TR = 1.5$ scenarios, while blocked culverts in the other scenarios cause

https://doi.org/10.5194/egusphere-2025-5228
Preprint. Discussion started: 25 November 2025

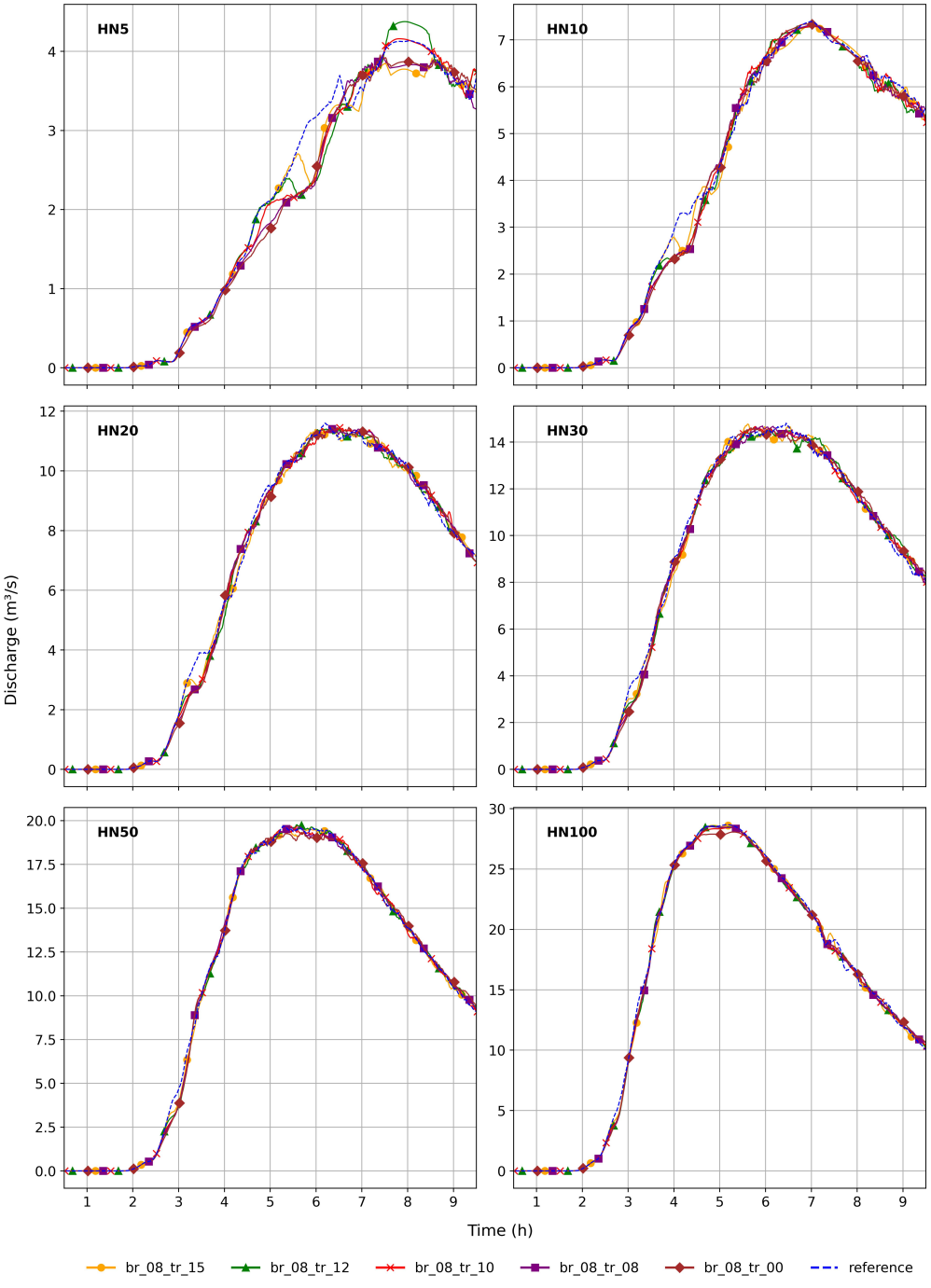

Figure 6. Outlet hydrographs for the different precipitation return periods and different TRs for $BR = 0.8$.

https://doi.org/10.5194/egusphere-2025-5228
Preprint. Discussion started: 25 November 2025

upstream retention and reduce peak flows. An exception is noted in the HN30 event for the $TR = 1.2$ scenario, where the timing of culvert blockage leads to an increase in peak discharge.

3. Cross-section 3 lies within the municipality of Reichenberg, where the Reichenberger Bach is fully routed underground. Consequently, any simulated discharge here indicates surcharge conditions due to culvert overloading. Given its relevance for urban flood risk, this cross-section is discussed in more detail later in this section.

4. Cross-section 4 is located upstream of a toward-stream culvert connecting the Sichelgrund to the Reichenberger Bach. Situated within the municipality of Reichenberg, this site is influenced by several upstream culverts, which are all blocked in higher return period scenarios. Nevertheless, the hydrographs show no substantial differences compared to the reference scenario, except for HN5, where minor timing variations in blockage initiation result in small retention effects during the rising limb.

5. Cross-section 5 lies upstream of Reichenberg along the Reichenberger Bach. Except for the HN5, only the HN50 and HN100 scenarios exhibit minor differences in peak discharge, with the initially blocked scenario producing slightly lower peaks. This suggests the presence of culverts upstream that are not blocked in the triggered scenarios but do reduce flow when blocked from the beginning.

6. Cross-section 6 is located further upstream on the Reichenberger Bach. Peak discharges here are less than half of those at cross-section 5. Similar to cross-section 5, culverts upstream are never blocked in the triggered scenarios but demonstrate an influence on hydrographs when initially blocked.

7. Cross-section 7 lies upstream of Reichenberg along the Guttenberger Bach. Only one upstream culvert, identified during the field campaign, is present. This culvert influences the hydrographs for HN50 and HN100 by reducing peak discharges. It is not blocked in any of the triggered scenarios.

Overall, cross-sections 2 and 5–7 illustrate that culvert blockages can induce localized retention effects within subcatchments. Particularly at cross-section 2, the simulated time of culvert blockage is shown to significantly influence peak discharge, with untimely blockage potentially amplifying the flood peak.

Cross-section 3 warrants special attention, as it is situated within the urban core of Reichenberg, where both the Reichenberger and Guttenberger Bachs are conveyed through underground pipes. Under dry weather conditions, no surface flow occurs at this location. Thus, any simulated discharge here reflects surcharge conditions and surface flooding due to culvert overloading. Figure 7 presents the hydrographs for all return periods across different blockage scenarios at this critical location.

- HN5:

  The HN5 event clearly illustrates how the triggered blockage of a critical culvert upstream of Reichenberg leads to significantly increased surface flooding within the municipality. In the initially blocked scenario, a sharp increase in discharge at cross-section 4 occurs at approximately $t = 4h$ closely followed by the $TR = 0.8$ scenario, which shows that

https://doi.org/10.5194/egusphere-2025-5228
Preprint. Discussion started: 25 November 2025

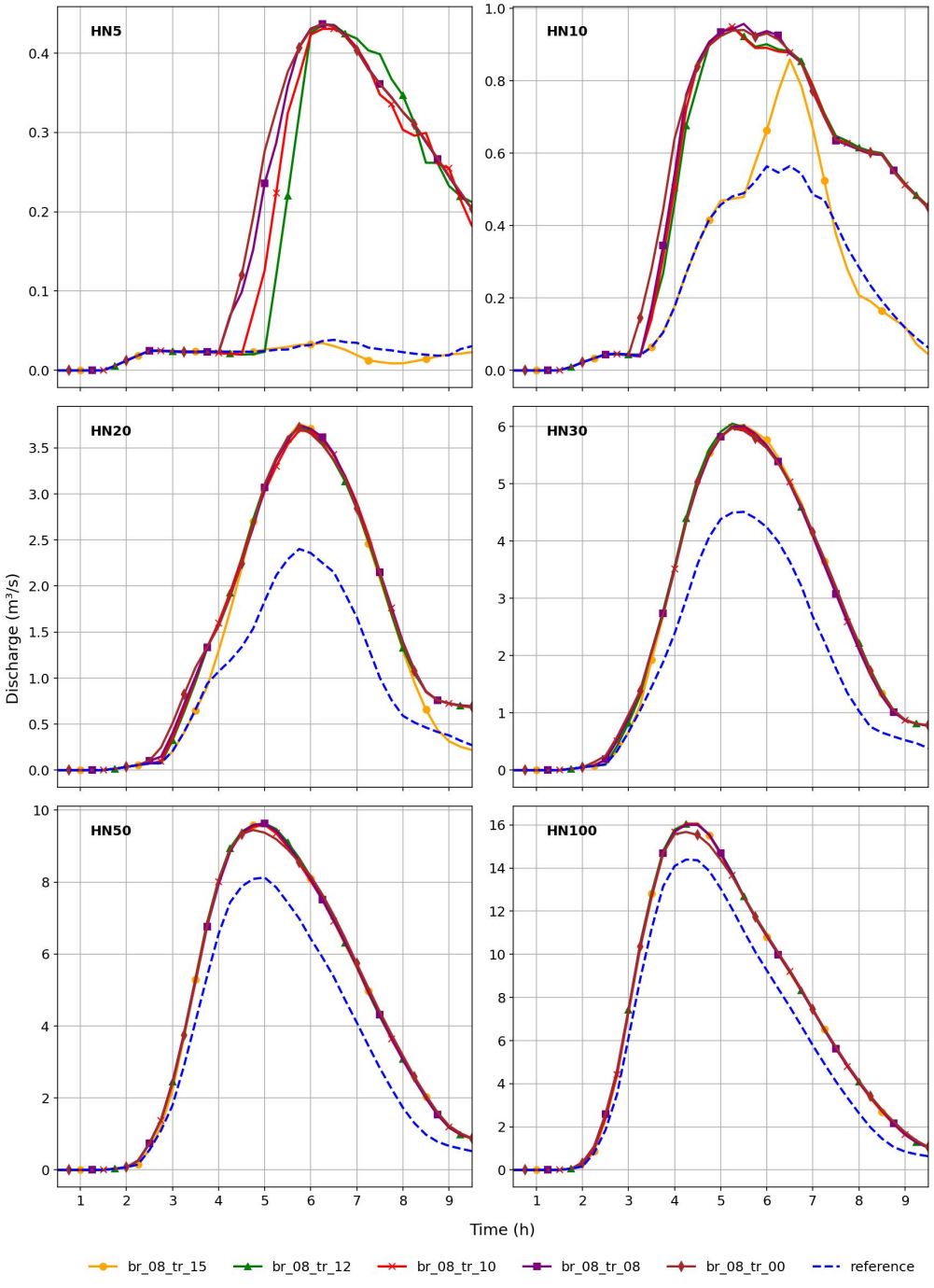

Figure 7. Hydrographs at cross-section 4 for the different precipitation return periods and different TRs for $BR = 0.8$.

https://doi.org/10.5194/egusphere-2025-5228
Preprint. Discussion started: 25 November 2025

the blockage with $TR = 0.8$ introduces only a slight delaya slight delay. The $TR = 1.0$ scenario exhibits a similar sharp increase a $t = 4.5h$, and the $TR = 1.2$ scenario follows at $t = 5h$.Notably, the $TR = 1.5$ scenario does not experience this rapid rise, resulting in considerably lower flooding, comparable to the reference scenario. In total, eight culverts experience triggered blockage in the $TR = 1.2$ scenario, compared to six in the $TR = 1.5$ scenario. One of the additionally blocked culverts in the $TR = 1.2$ scenario is located just downstream of cross-section 4. Once blocked, excess water unable to pass through this culvert is diverted directly through the urban area of Reichenberg. This identifies the culvert as a hydraulically critical structure with direct influence on cross-section 3 and, by extension, making a the difference between flooding and no flooding in Reichenberg for small return periods.

- HN10:

  During the HN10 event, culverts upstream of Reichenberg are already overloaded in the reference scenario, resulting in increased urban discharge even without explicit blockage. In the blockage scenarios ($TR = 0$, $TR = 0.8$, $TR = 1.0$, and $TR = 1.2$), the critical culvert downstream of cross-section 4 becomes blocked between $t = 3h$ and $t = 3.5h$, causing a substantial increase in discharge. In contrast, the $TR = 1.5$ scenario does not trigger a blockage of this culvert until $t = 5.5h$, resulting in a delayed and slightly attenuated discharge response. Nonetheless, the peak discharge in the $TR = 1.5$ scenario remains lower than in the other blockage scenarios, in which the peaks nearly double that of the reference scenario.

- HN20:

  For the HN20 event, the difference in the timing of the rapid discharge increase between the $TR = 1.5$ and other blockage scenarios is less pronounced, indicating that the blockage of the critical culvert now occurs less time-delayed across scenarios. As a result, both the timing and magnitude of the peak discharge are nearly identical in all blockage scenarios, though the relative difference from the reference scenario has decreased.

- HN30:

  In the HN30 event, all blockage scenarios produce nearly identical hydrographs. This convergence is due to the simultaneous triggering of blockages in the most influential culverts. The relative difference between the blockage scenarios and the reference scenario continues to decrease, as culvert overloading becomes increasingly dominant even in the absence of explicit blockage.

- HN50:

  For HN50, the hydrographs remain nearly indistinguishable across all blockage scenarios. Only the initially blocked scenario shows a slightly attenuated discharge peak. The gap between the blockage scenarios and the reference scenario narrows further, indicating a diminishing influence of blockage on the flood dynamics.

- HN100:

https://doi.org/10.5194/egusphere-2025-5228
Preprint. Discussion started: 25 November 2025

In the HN100 event, the discharge peak in the initially blocked scenario is even more flattened compared to the HN50 case. The hydrograph of the reference scenario more closely aligns with those of the blockage scenarios, signifying that flooding due to culvert overloading now almost matches the contribution of culvert blockage. While the overall extent of inundation is greatest for the HN100 event, the relative difference in inundation between the reference and blockage scenarios is the smallest across all analyzed return periods.

Overall, the relative difference in peak discharge between the blockage scenarios and the reference scenario is more pronounced for lower return periods, when the blockage of critical culverts is triggered. This highlights the major influence that certain culverts can exert on flood dynamics, thus offering a valuable opportunity for targeted flood mitigation. Through detailed analysis of culvert blockage scenarios within flood models, it is possible to identify particularly crucial culverts whose continued function is essential during flood events. Preventive measures—such as debris clearance, structural reinforcements, or real-time monitoring—can then be prioritized for these culverts both prior to and during flood events. This approach will be further discussed in Section 3.5.

The timing of blockage initiation, governed by the trigger ratio (TR), is also a key factor. For lower return periods, culvert blockages may not be triggered at all, and the culverts remain fully operational. However, accurately determining the trigger point of blockage is inherently challenging, as it depends on multiple interrelated factors, including upstream water levels, the presence of debris or woody material, and complex local inflow dynamics. In this study, blockage has been modeled as an instantaneous event, a simplification adopted to avoid further complicating the simulation with dynamic or progressive blockage processes.

3.4 Impact of Blocked Culverts on Inundation

Culvert blockages can lead to increased inundation both upstream of the culvert inlet and downstream, particularly if the embankment or structure the culvert traverses (e.g., roads, railway embankments) is overtopped. Figure 8 illustrates the maximum water depths in Reichenberg for the HN5 event, once without modelled blockage (A), and once with modelled blockages applying $BR = 0.8$ and $TR = 1.2$ (B). Additionally, the absolute increase in maximum water depth due to blockage is highlighted (C).

As the investigated catchment is steep, only minor differences can be noticed in the inundation extents from the maximum water depths. However, the difference in the maximum water depths illustrates that the increase in water depth is significant.

Increased inundation does not necessarily increase the induced damage by the flood. Therefore, it is important to analyse at which land use categories the increased inundation is located. To assess this, the study not only evaluates the overall change in inundation due to culvert blockages but also quantifies the impact on specific land use categories, namely streets and combined residential and industrial (resind) areas. As higher water depths are also linked to greater damage (Molinari et al., 2020; Wing et al., 2020), the analysis in this section focuses on inundated areas with water depths exceeding 30 cm to emphasize hazardous conditions. Figure 9 illustrates the relative differences in inundated area for the total domain and for the selected land use classes across multiple return periods. All blockage scenarios use a trigger ratio of $TR = 0.8$ but vary the blockage ratio

https://doi.org/10.5194/egusphere-2025-5228
Preprint. Discussion started: 25 November 2025

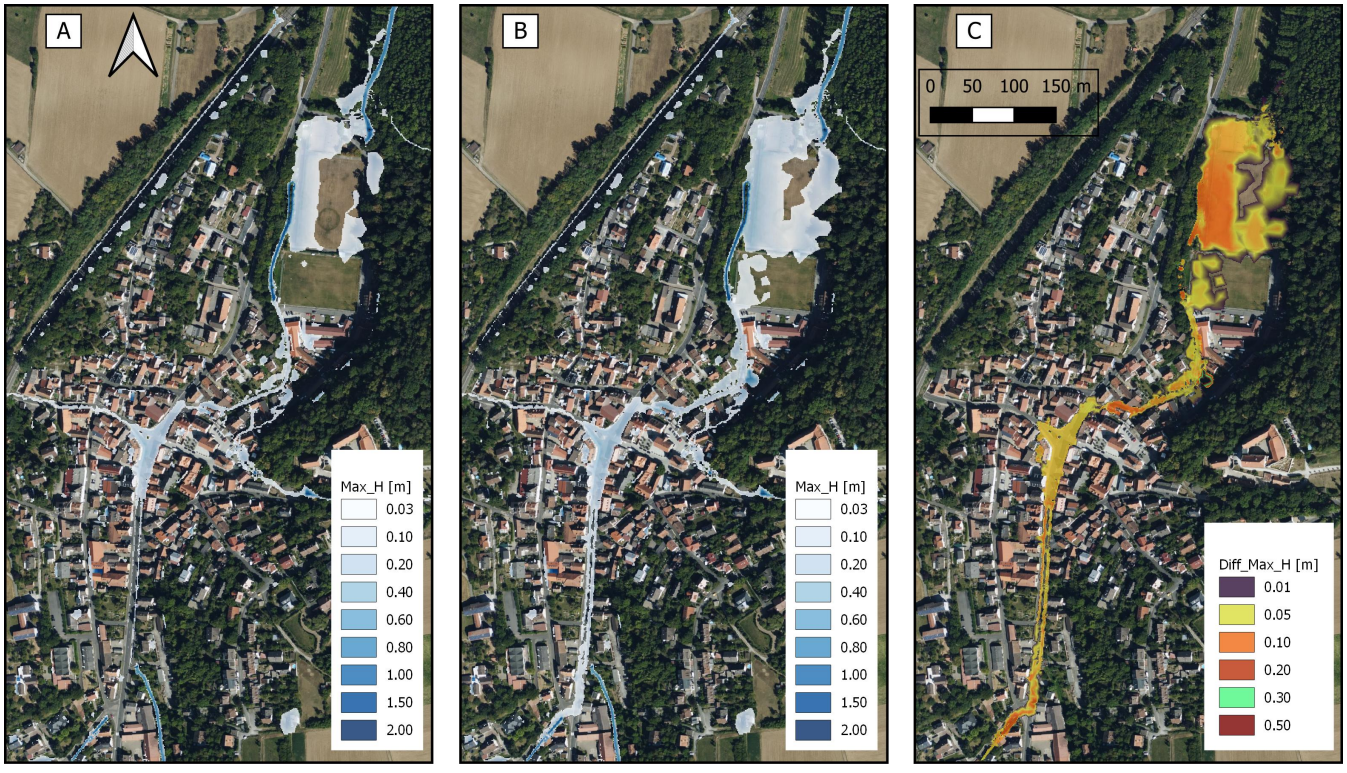

Figure 8. A: Maximum water depth ($\mathrm{Max_H}$) for an HN5 event without simulated blockage. B: Maximum water depth for an HN5 event with a blockage scenario applying $BR = 0.8$ and $TR = 1.2$. C: Difference in maximum water depth between the HN5 event with modelled blockage and without blockage. Basemaps: Bing Maps © Microsoft Corporation and its data providers.

($BR = 0.8$, 0.5, and 0.2). Thus, the number of blocked culverts remains constant, while the severity of each blockage varies, affecting upstream water levels differently. The underlying data are provided in Appendix B, Table B1.

Scenarios with $BR = 0.8$ produce the most substantial increases in inundation. While the total inundated area increases by only between 1% and 3%, the inundation increase in critical areas is considerably higher. Streets experience increases exceeding 10% for the return periods lower than HN30, and resind areas show similar increases for HN20 and HN30. Notably, the additional relative increase in inundation in streets is highest for the HN5 event and then decreases steadily through HN100. In contrast, peak relative increase inundation in resind areas occurs during the HN20 event and diminishes for higher return periods.

The $BR = 0.5$ scenarios exhibit significantly lower impacts. Across all return periods, the total increase in inundated area remains below 1.2%. The temporal trends are consistent with the $BR = 0.8$ scenarios, though the maximum inundation increase in resind areas now occurs at HN5 rather than HN20. For HN100, inundation in these areas actually decreases minimally relative to the reference scenario.

https://doi.org/10.5194/egusphere-2025-5228
Preprint. Discussion started: 25 November 2025

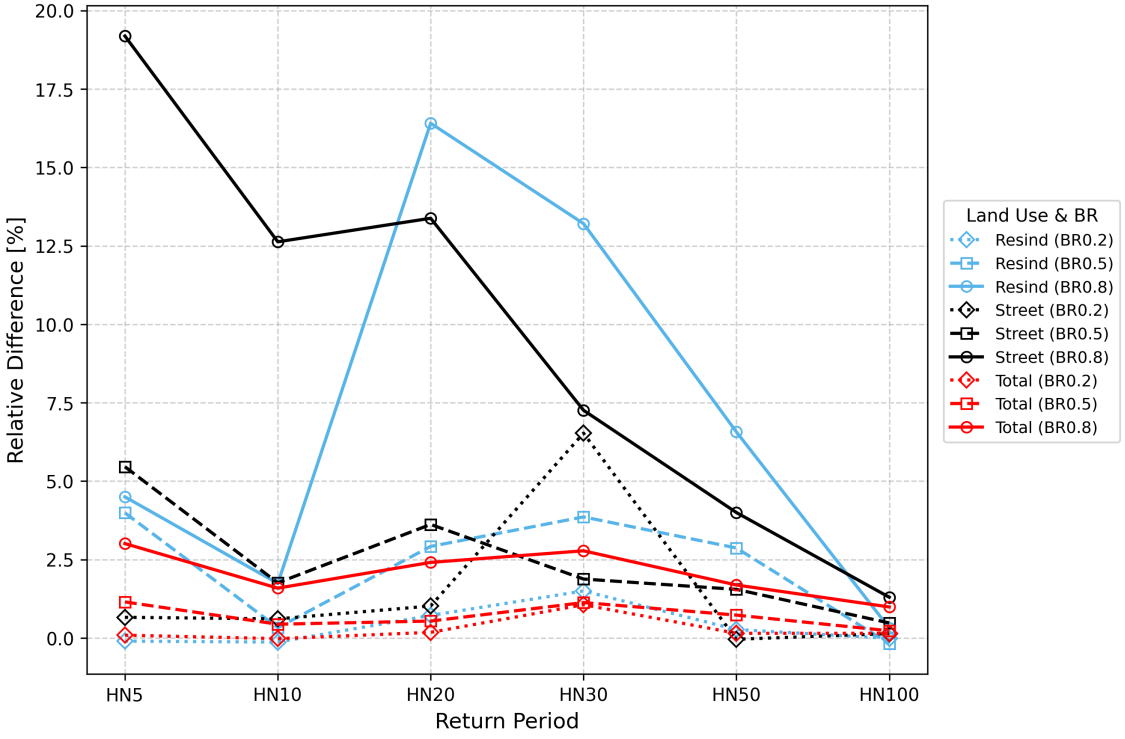

Figure 9. Relative difference of inundation area with water depth greater than 30 cm between blockage scenarios with constant $TR = 1.2$, but variable BR and the reference scenarios across multiple return periods. The relative difference is given for the land uses streets and combined residential and industrial (resind) areas, as well as total inundation.

In the $BR = 0.2$ scenario, inundation increases are negligible. Outside of HN30, total and land use-specific inundation changes remain below 1%, with some scenarios even showing a very small reduction in inundated area. The HN30 event stands out as an outlier, exhibiting disproportionately large increases that deviate from the general pattern and are likely attributable to numerical instabilities or oscillations in the model simulation.

Figure 10 presents the inundation increase analysis for varying trigger ratios ($TR = 0.0$, 0.8, 1.0, 1.2 and 1.5), while maintaining a constant blockage ratio of $BR = 0.8$. Due to the varying trigger ratios, the number and timing of culvert blockages differ across scenarios. The underlying data are provided in Appendix B, Table B2.

For events with lower return periods, triggered blockages show larger increases in relative inundation. In the HN5 event, the inundation in streets increases by almost 20 %. However, defining a trigger ratio $TR = 1.5$, there is only a low increase in inundation by 1.4 %. This indicates again that a critical culvert remains unblocked in this scenario, but is blocked in the other scenarios with lower TRs. In general, the inundation in the streets decreases for higher return periods and becomes almost insignificant for the HN100. Only for the $TR = 1.5$ scenario, the largest relative inundation increase is around the HN20 and HN30 event, indicating that the critical culvert has the largest impact for these return periods.

https://doi.org/10.5194/egusphere-2025-5228
Preprint. Discussion started: 25 November 2025

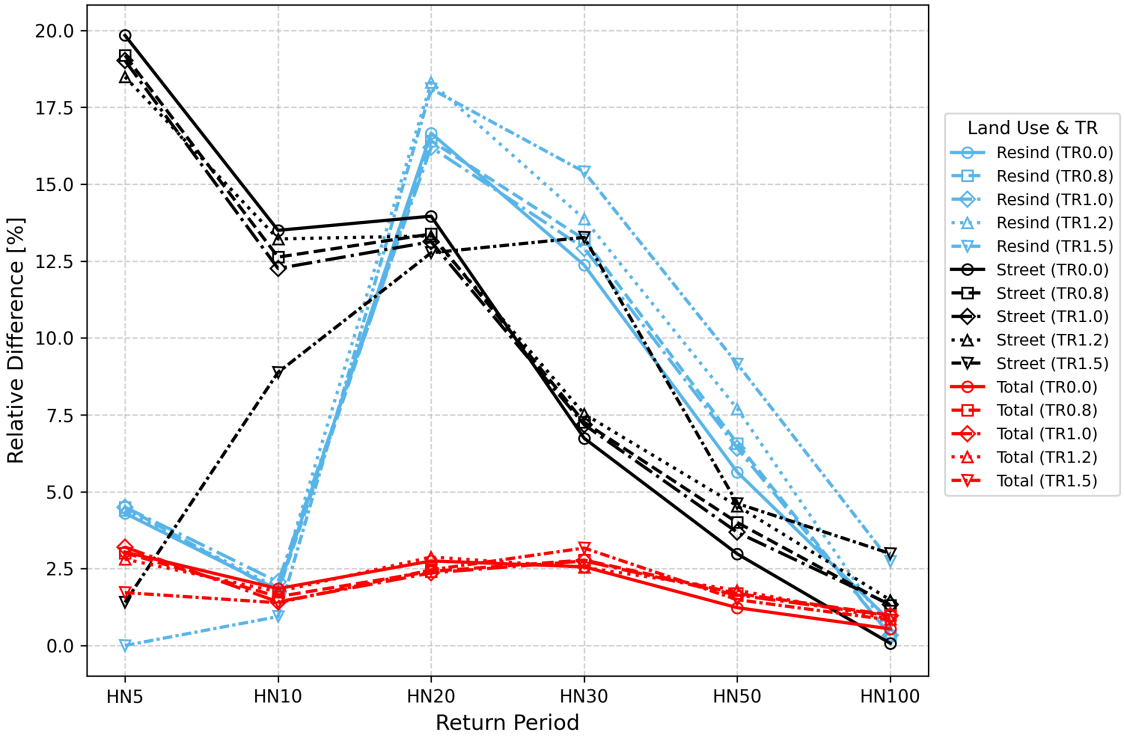

Figure 10. Relative difference of inundation area with water depth greater than 30 cm between blockage scenarios with constant $BR = 0.8$, but variable TR and the reference scenarios across multiple return periods. The relative difference is given for the land uses streets and combined residential and industrial (resind) areas, as well as total inundation.

For resind areas, the largest relative increases in inundation are for the HN20 return period, pointing to a critical culvert getting blocked only for events larger than HN20. The relative increase in inundation in resind areas then decreases with higher return periods, once again being almost insignificant for the HN100 return period.

In general, the results indicate that at lower return periods, lower trigger ratios lead to greater relative increases in inundation. However, at higher return periods, higher trigger ratios result in a more pronounced effect, since the delayed blockage is closer to the overall flood peak. The increases in inundation diminish for the HN50 and HN100, as culverts are already overwhelmed in the reference scenario and the extent of flooding is large regardless of blockage timing.

3.5 Simulation and Designing of Mitigation Measure

The analyses in sections 3.3 and 3.4 enable the identification of critical culverts within the study area. By varying the trigger ratios and return periods, locations exhibiting abrupt increases in inundation can be detected. A comparison of scenarios with significant inundation increases against those with minimal changes reveals a set of culverts that are potential drivers of the observed differences. Culverts that are part of this candidate group but located further away from the affected areas are

https://doi.org/10.5194/egusphere-2025-5228
Preprint. Discussion started: 25 November 2025

less likely to be critical. To further narrow down the set of critical culverts, discharge through cross-sections near regions of increased inundation is analyzed. The timing of culvert blockages is extracted from the simulation data. If a distinct change in discharge is observed in the vicinity of a culvert shortly after its blockage, a direct influence on local flow conditions can be inferred. Complementary to this, a visual assessment of the spatiotemporal inundation patterns supports the identification of culverts that critically affect flood dynamics.

Based on these analyses and using Figure 7 and the previously described method, two critical culverts within the study area were identified (see Figure 1). To further assess their influence on inundation dynamics, three additional scenarios were defined in which one (cc1 or cc2)or both (cc1,2) of these culverts were exempted from blockage by assigning them an infinite trigger ratio ($TR = \infty$). This configuration represents the implementation of a mitigation measure during the flood event, such as the manual removal of debris by emergency services. For all other culverts, a trigger ratio of $TR = 1.2$ and a blockage ratio of $BR = 0.8$ were applied. Figure 11 compares the resulting inundation extents from these simulated mitigation scenarios with those of the corresponding baseline scenarios lacking such interventions ("no mitig"). The underlying data of Figure 11 is provided in Appendix B, Table B3

In the HN5 event, the simulated mitigation measure at critical culvert 1 (cc1) nearly eliminates the increased inundation observed in streets (from 18.49 % to 1.40 %) and residential areas (from 4.40 % to 0.10 %). In contrast, preventing blockage at critical culvert 2 alone (cc2) has negligible impact. The combined mitigation of both culverts (cc1,2) yields only a marginal improvement over solely prohibiting blockage at culvert 1, indicating that blocked culvert 1 is the dominant contributor to indundation in the HN5 event and a blockage mitigation measure here is most effective, whereas culvert 2 exhibits limited sensitivity to the inundation dynamics.

For the HN10 event, prohibiting blockage at culvert 1 reduces the inundation increase to 8.77 %. Interestingly, preventing blockage only at culvert 2 slightly increases the inundation to 13.48 %, suggesting potential redistribution effects. However, when blockage is prohibited at both culverts, the inundation increase drops significantly to 1.76 %, indicating that both culverts are hydraulically influential during this event—despite culvert 2 having no mitigating effect when considered in isolation.

At higher return periods (HN20 to HN100), culvert 2 emerges as the more critical structure. While mitigation at culvert 1 alone results in only minor improvements, preventing blockage at culvert 2 consistently leads to substantial reductions in inundation extent across these scenarios.

These findings highlight the importance of targeted mitigation strategies focused on hydraulically critical culverts. However, the criticality of individual culverts is not constant across return periods. A culvert may play a negligible role during low-magnitude events but become a key factor in mitigating flooding under more extreme conditions. Hydrodynamic modeling of different culvert blockage scenarios is therefore a valuable tool to identify critical culverts and to design effective mitigation measures against increased inundation due to blockage.

3.6 Limitations

The primary limitation of this study lies in the inability to robustly validate the hydrodynamic model and the subsequent findings of the blockage modeling. A plausibility check was conducted using photographs from a reference flood event and a

https://doi.org/10.5194/egusphere-2025-5228
Preprint. Discussion started: 25 November 2025

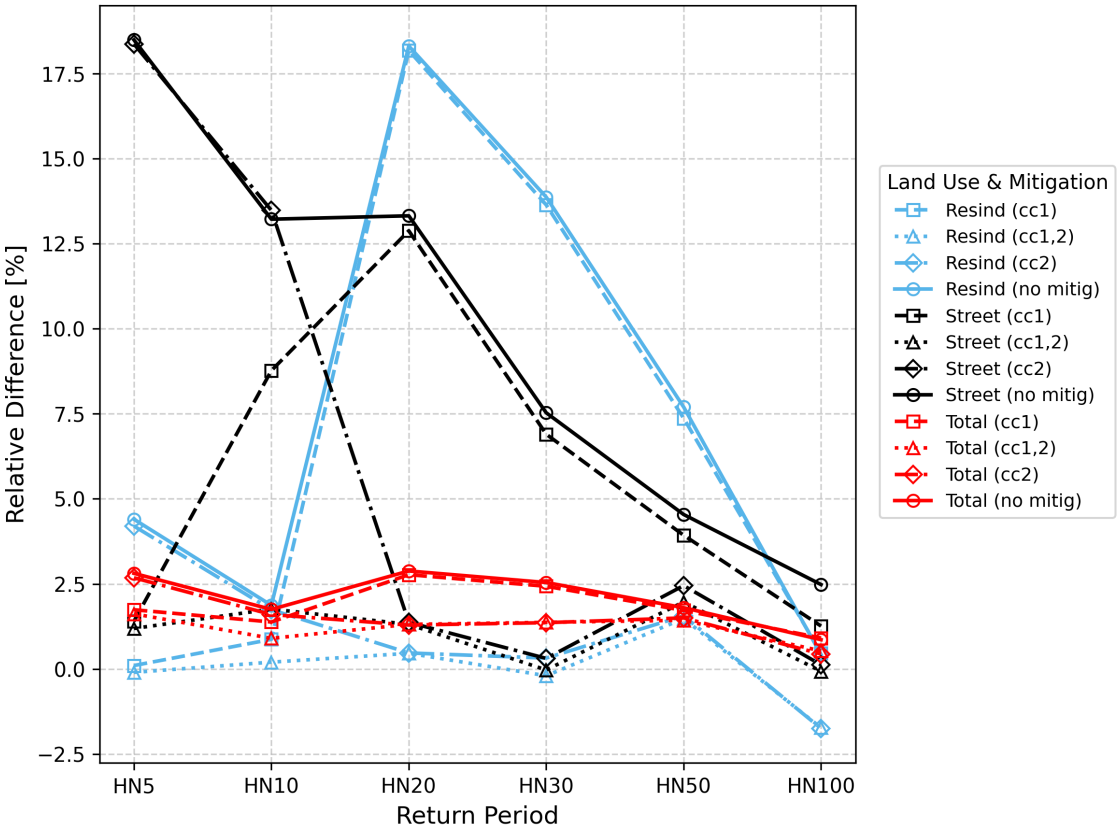

Figure 11. Relative difference of inundation area with water depth greater than 30 cm between blockage scenarios and the reference scenarios across multiple return periods. These blockage scenarios share the same blockage ratios $BR = 0.8$ and trigger ratios $TR = 1.2$, except for the scenarios in which installed mitigation measures are simulated at the critical culverts 1 (cc1), 2 (cc2) or both (cc1,2) by applying $TR = \infty$. The relative difference is given for the land uses streets and combined residential and industrial (resind) areas, as well as total inundation.

water mask derived from a field campaign. It is true that hydrodynamic models for short-duration, high-intensity precipitation events are rarely amenable to full calibration. Yet, as demonstrated by (Apel et al., 2008), they offer valuable insights into flood dynamics and can be used advantageously for supporting the planning of mitigation strategies. Research specifically addressing culvert blockages during flood events remains limited, as the majority of studies focuses on debris accumulation at bridges, probably also due to better data availability. Well aware of the described limitations, the present study employs a state-of-the-art culvert blockage model (Ollett et al., 2017) and yields robust findings by simulating a wide range of precipitation and blockage scenarios.

Within the blockage modeling, the main factor of uncertainty stems from the timing and degree of culvert blockage. This study has assumed instantaneous blockage rather than gradual accumulation. While continuous blockage functions were implemented into the model, the associated increase in parameter complexity led to a focus on scenario-based analysis with

https://doi.org/10.5194/egusphere-2025-5228
Preprint. Discussion started: 25 November 2025

varying trigger and blockage ratios only. To the authors' knowledge, gradual culvert blockages have not yet been thoroughly investigated in the literature. The only comparable study found, by Ah-Woane et al. (Ah-Woane et al., 2025), also adopts an instantaneous blockage approach, triggered by global maximum flood parameters.

The degree of inundation increase caused by culvert blockage, as identified in this study, is inherently catchment-specific. Variations in topography, land use, and hydraulic infrastructure strongly influence the sensitivity and impact of blocked culverts, particularly in vulnerable areas. Nevertheless, this study demonstrates the necessity of explicitly representing all culverts in a catchment for accurate flood modeling. It shows that the blockage of individual critical culverts can substantially increase inundation and, consequently, damage potential. Furthermore, it highlights that scenario-based analyses, accounting for multiple return periods and blockage parameters, enable the identification of critical culverts and the design of effective mitigation strategies.

This work exclusively focuses on culverts and does not examine the impact of blocked bridges. Although numerous bridges are present in the study area, their influence on inundation is generally limited by their structural geometry: backwater effects tend to be constrained by the bridge thickness. Only dense and voluminous blockage formations, exceeding the bridge height, could result in significant upstream inundation. As such, the contribution of bridge blockages to inundation in this context is expected to be minor.

Finally, one of the most severe hazards associated with culvert blockages is the potential failure of the culvert structure itself, leading to the erosion of the topographic dam. This can result in the abrupt release of impounded water, combined with sediment and debris, potentially triggering catastrophic downstream impacts. Modeling such dam-break processes would introduce additional parameters, sensitivities, and uncertainties, and was therefore excluded from this study. However, given the severity of this hazard, this study strongly cautions against the deliberately inducing blockage to reduce discharge as a basis for mitigation planning. Debris and other potentially obstructive materials in front of culverts should always be removed promptly to ensure culvert functionality.

4 Conclusion

This study has demonstrated the importance of incorporating a comprehensive culvert dataset in catchment-scale flash flood modeling, particularly when assessing the impacts of culvert blockages. The results show that certain culverts can exert an large influence on flood dynamics, underlining the need to identify and prioritize these critical structures. By applying a scenario-based modeling approach with varying degrees and timings of culvert blockage, this study provides a solid framework for evaluating the effectiveness of targeted mitigation strategies, given that blockage information is simply not available. Analyses results can be directly provided to emergency planning and flood risk management, particularly first responders. Consequently, accounting for culvert blockages should become an integral part of flash flood modeling and hazard assessment. The foundation for this work must be a detailed culvert data set and a refined culvert modeling framework.

Future research should further investigate the processes driving culvert blockage formation. Laboratory experiments can provide insight into blockage mechanisms and thresholds, which could then be translated into dynamic numerical models.

https://doi.org/10.5194/egusphere-2025-5228
Preprint. Discussion started: 25 November 2025

Moreover, there remains a significant gap in the availability and accuracy of field data—not only concerning blockage occurrence during flash flood events but also regarding the geometric detail and spatial accuracy of culvert infrastructure. Bridging this data gap is essential for improving model reliability and enhancing risk-informed flood management practices.

https://doi.org/10.5194/egusphere-2025-5228
Preprint. Discussion started: 25 November 2025

Appendix A: Hydrographs at different Cross-sections throughout the Catchment

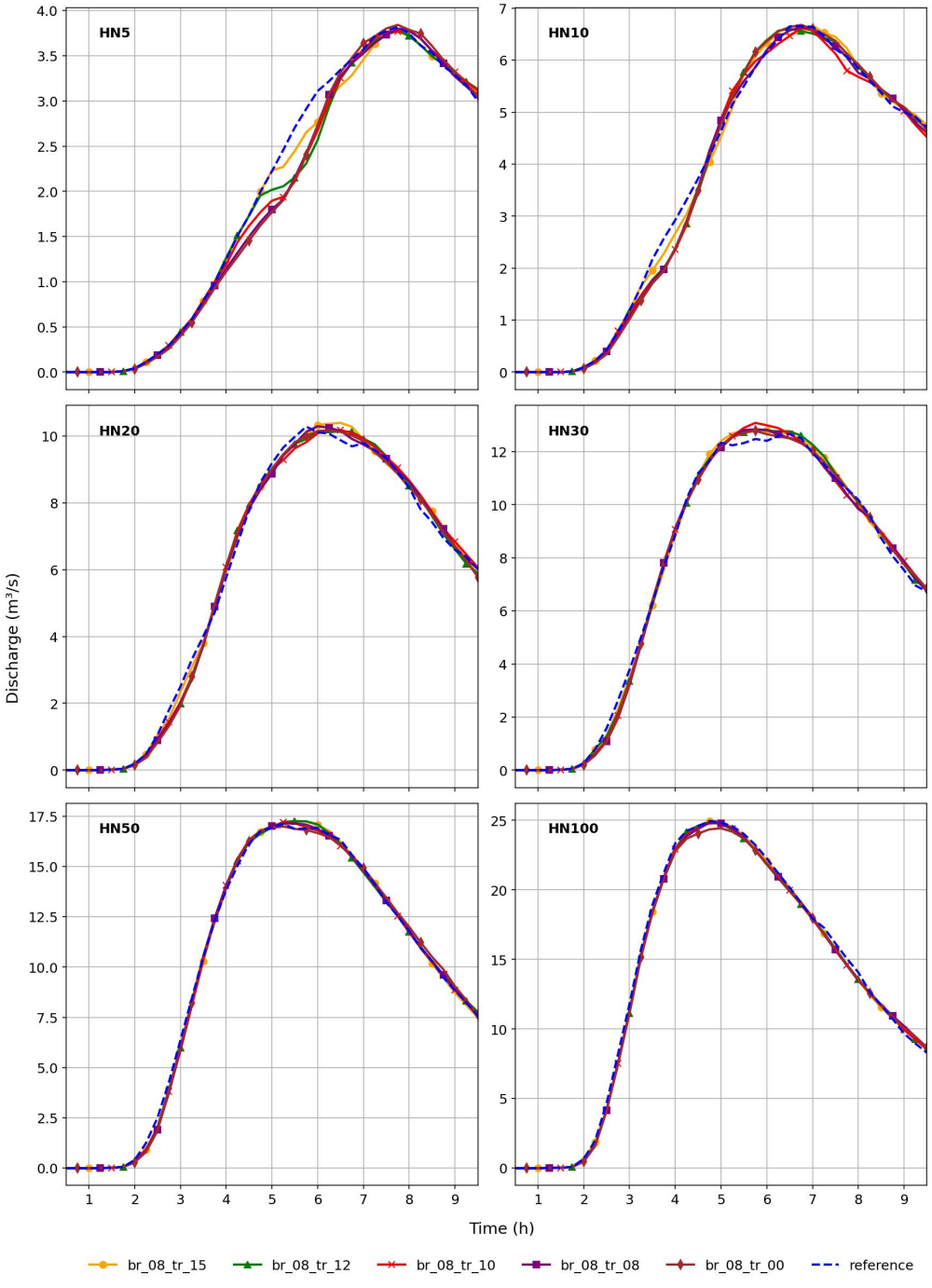

Figure A1. Hydrographs at cross-section 1 for the different precipitation return periods and different TRs for $BR = 0.8$.

https://doi.org/10.5194/egusphere-2025-5228
Preprint. Discussion started: 25 November 2025

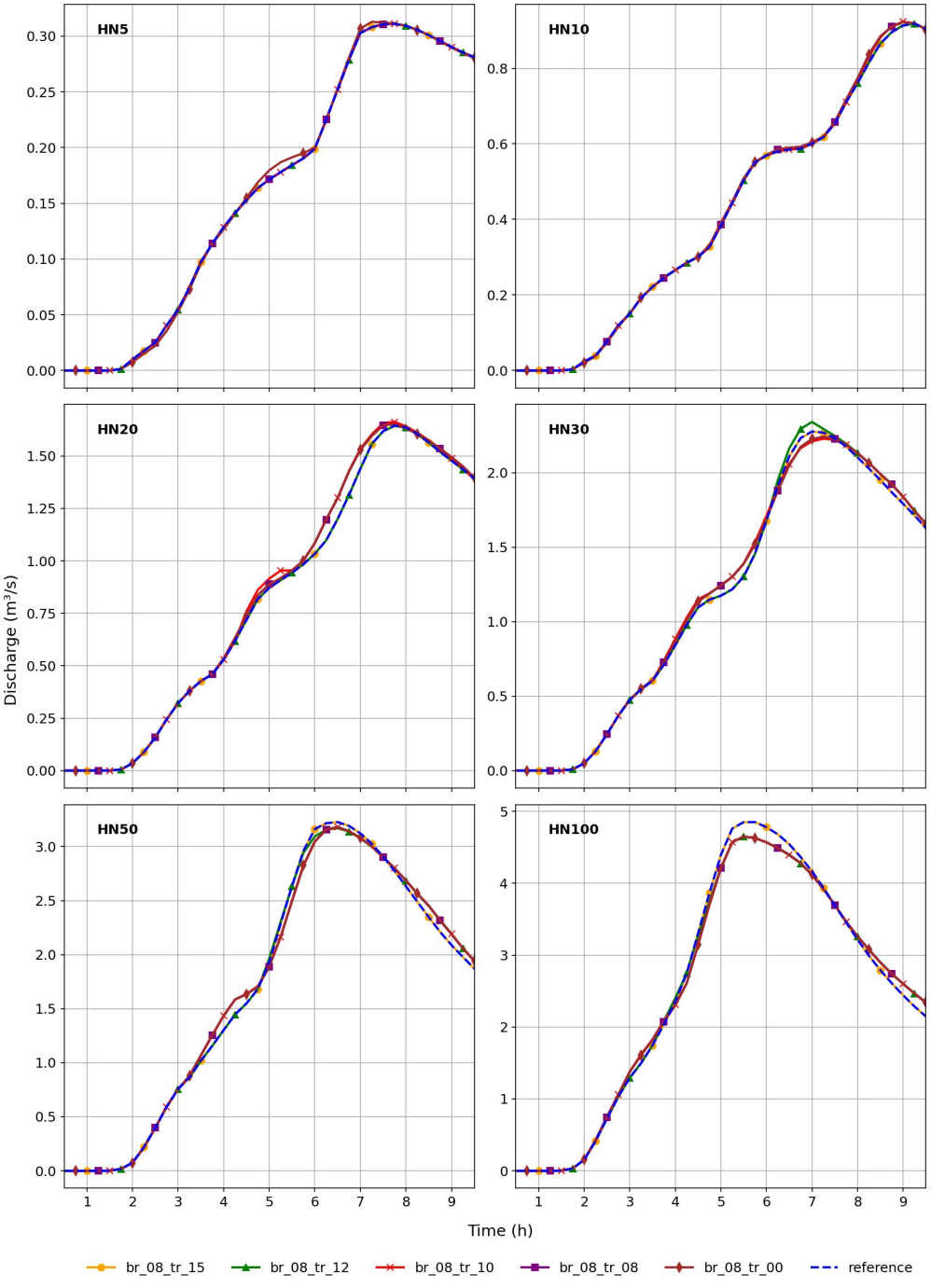

Figure A2. Hydrographs at cross-section 2 for the different precipitation return periods and different TRs for $BR = 0.8$.

https://doi.org/10.5194/egusphere-2025-5228
Preprint. Discussion started: 25 November 2025

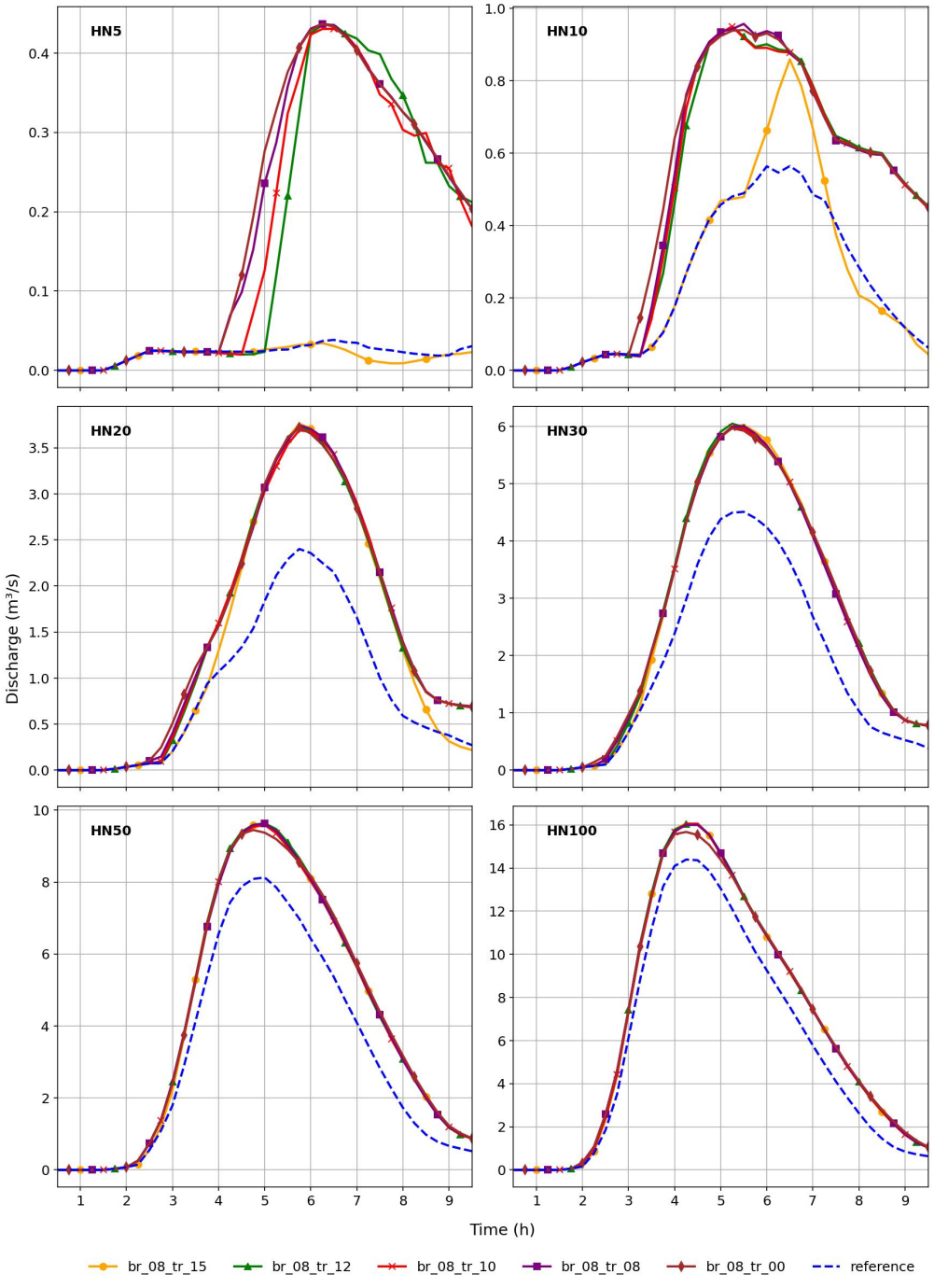

Figure A3. Hydrographs at cross-section 3 for the different precipitation return periods and different TRs for $BR = 0.8$.

https://doi.org/10.5194/egusphere-2025-5228
Preprint. Discussion started: 25 November 2025

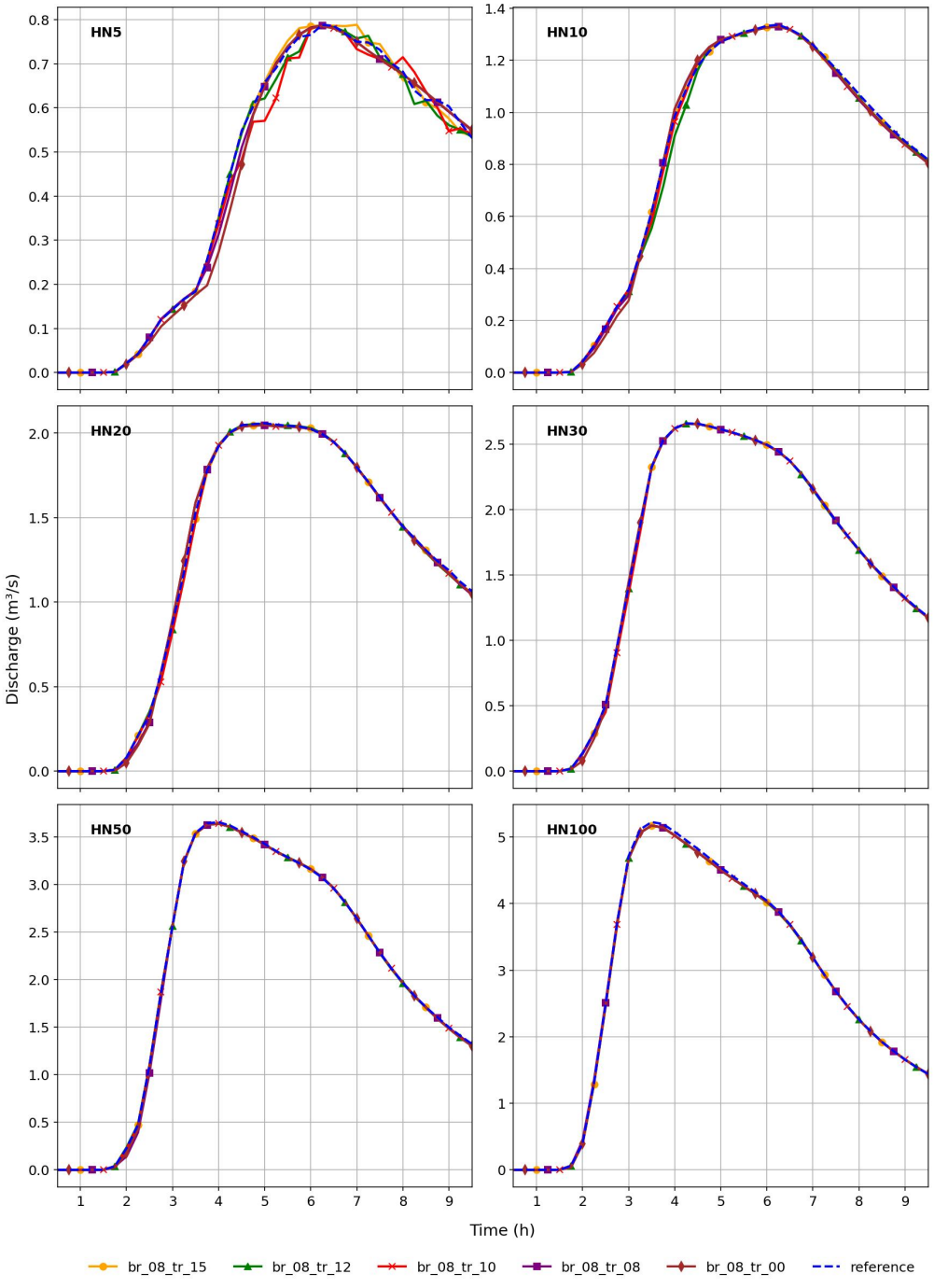

Figure A4. Hydrographs at cross-section 4 for the different precipitation return periods and different TRs for $BR = 0.8$.

https://doi.org/10.5194/egusphere-2025-5228
Preprint. Discussion started: 25 November 2025

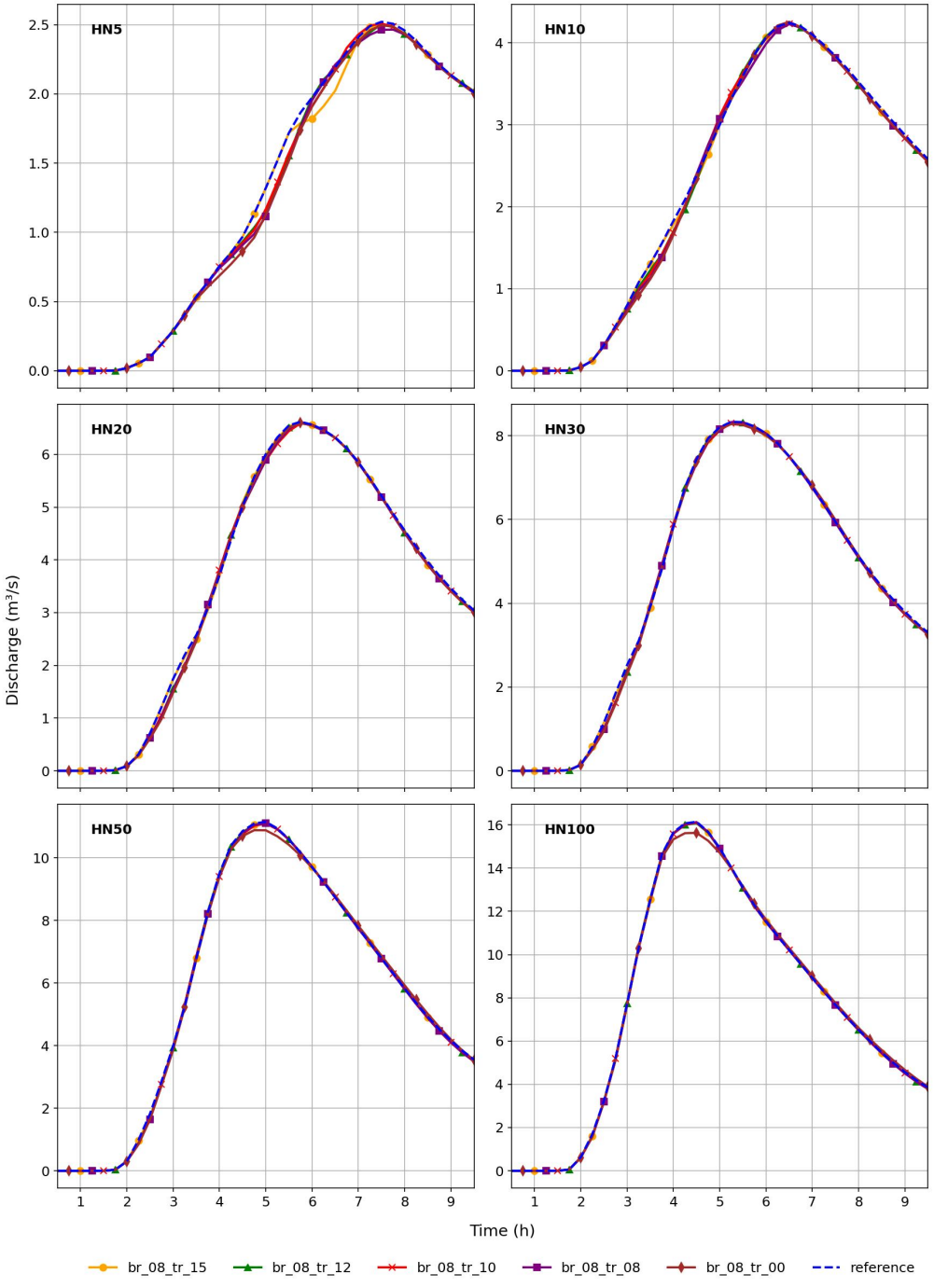

Figure A5. Hydrographs at cross-section 5 for the different precipitation return periods and different TRs for $BR = 0.8$.

https://doi.org/10.5194/egusphere-2025-5228
Preprint. Discussion started: 25 November 2025

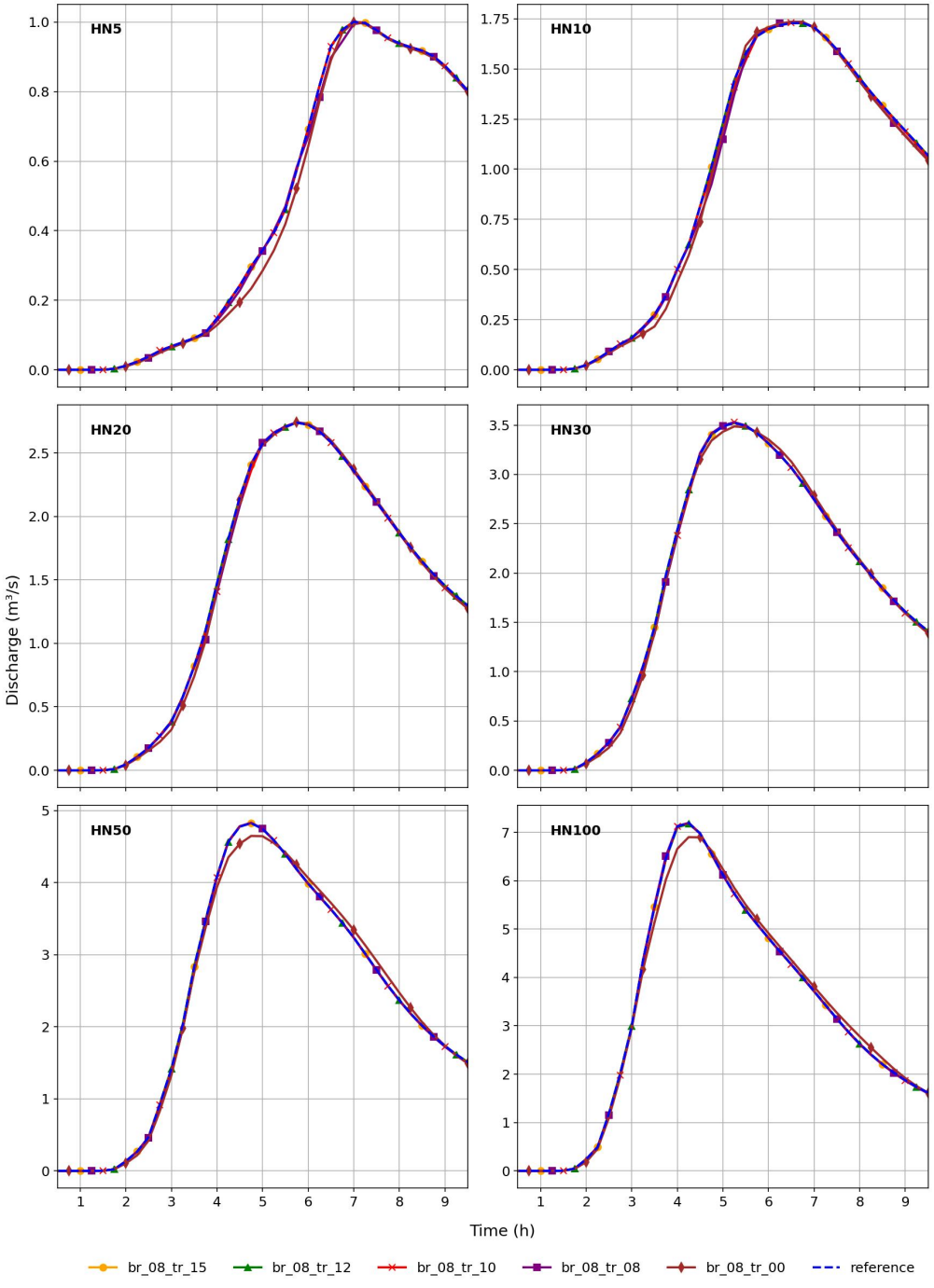

Figure A6. Hydrographs at cross-section 6 for the different precipitation return periods and different TRs for $BR = 0.8$.

https://doi.org/10.5194/egusphere-2025-5228
Preprint. Discussion started: 25 November 2025

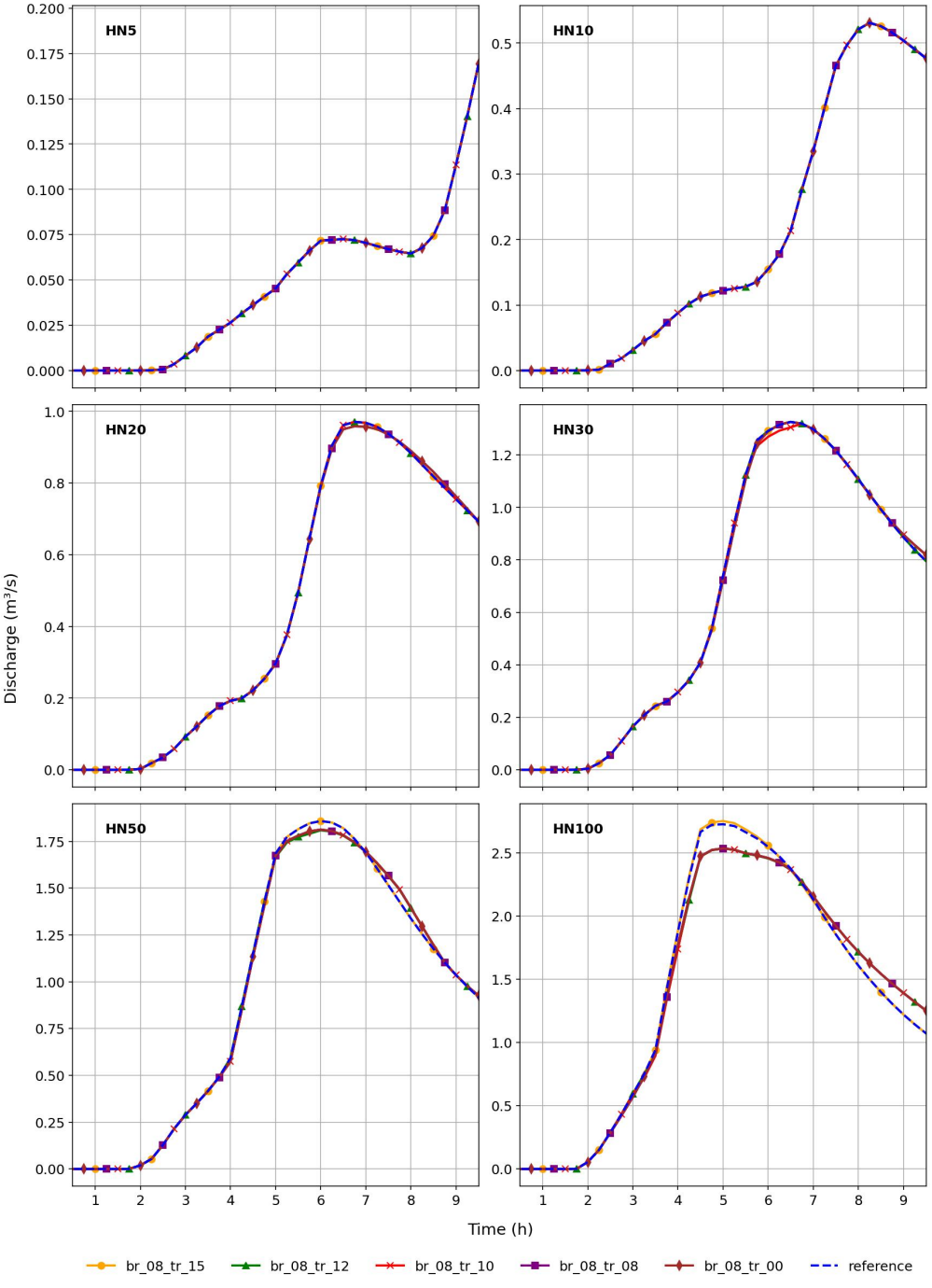

Figure A7. Hydrographs at cross-section 7 for the different precipitation return periods and different TRs for $BR = 0.8$.

https://doi.org/10.5194/egusphere-2025-5228
Preprint. Discussion started: 25 November 2025

Appendix B: Inundation area tables

Table B1. Absolute inundation larger than 30 cm in streets and combined residential and industrial (resind) areas, as well as total inundation for the reference scenario. The relative difference in inundation of three different blockage scenarios is listed as comparison. These blockage scenarios share the same trigger ratio $TR = 0.8$, but differ in blockage ratios BR.

		HN5	HN10	HN20	HN30	HN50	HN100
Reference, area with absolute inundation > 30 cm [m^2]	Street	2434	4266	8402	11726	17803	26299
	Resind	977	1495	2365	3468	5263	8248
	Total	57117	82445	112880	137398	178906	250673
BR=0.8, TR=0.8, relative diff. [%]	Street	19.19%	12.63%	13.38%	7.26%	4.00%	1.30%
	Resind	4.50%	1.74%	16.41%	13.21%	6.57%	0.32%
	Total	3.01%	1.59%	2.41%	2.78%	1.69%	0.99%
BR=0.5, TR=0.8, relative diff. [%]	Street	5.46%	1.76%	3.62%	1.88%	1.55%	0.48%
	Resind	3.99%	0.33%	2.92%	3.86%	2.87%	-0.18%
	Total	1.15%	0.44%	0.54%	1.13%	0.73%	0.23%
BR=0.2, TR=0.8, relative diff. [%]	Street	0.66%	0.61%	1.02%	6.53%	-0.04%	0.14%
	Resind	-0.10%	-0.13%	0.72%	1.50%	0.27%	-0.01%
	Total	0.09%	-0.02%	0.18%	1.06%	0.15%	0.15%

https://doi.org/10.5194/egusphere-2025-5228
Preprint. Discussion started: 25 November 2025

Table B2. Absolute inundation larger than 30 cm in streets and combined residential and industrial (resind) areas, as well as total inundation for the reference scenario. The relative difference in inundation of five different blockage scenarios is listed as comparison. These blockage scenarios share the same blockage ratios $BR = 0.8$, but differ in the trigger ratio TR.

		HN5	HN10	HN20	HN30	HN50	HN100
Reference, area with absolute inundation > 30 cm [m^2]	Street	2434	4266	8402	11726	17803	26299
	Resind	977	1495	2365	3468	5263	8248
	Total	57117	82445	112880	137398	178906	250673
BR=0.8, TR=0.0, relative diff. [%]	Street	19.84%	13.50%	13.96%	6.74%	2.98%	0.07%
	Resind	4.30%	1.81%	16.66%	12.37%	5.64%	0.80%
	Total	3.04%	1.85%	2.75%	2.56%	1.23%	0.54%
BR=0.8, TR=0.8, relative diff. [%]	Street	19.19%	12.63%	13.38%	7.26%	4.00%	1.30%
	Resind	4.50%	1.74%	16.41%	13.21%	6.57%	0.32%
	Total	3.01%	1.59%	2.41%	2.78%	1.69%	0.99%
BR=0.8, TR=1.0, relative diff. [%]	Street	19.02%	12.26%	13.13%	7.18%	3.68%	1.33%
	Resind	4.50%	2.07%	16.20%	12.92%	6.42%	0.33%
	Total	3.20%	1.42%	2.36%	2.75%	1.64%	0.97%
BR=0.8, TR=1.2, relative diff. [%]	Street	18.49%	13.22%	13.32%	7.53%	4.54%	1.48%
	Resind	4.40%	1.87%	18.31%	13.87%	7.70%	0.42%
	Total	2.81%	1.75%	2.88%	2.54%	1.80%	0.86%
BR=0.8, TR=1.5, relative diff. [%]	Street	1.40%	8.88%	12.77%	13.27%	4.62%	2.99%
	Resind	0.00%	0.94%	18.10%	15.40%	9.16%	2.74%
	Total	1.72%	1.39%	2.46%	3.17%	1.49%	0.83%

https://doi.org/10.5194/egusphere-2025-5228
Preprint. Discussion started: 25 November 2025

Table B3. Absolute inundation larger than 30 cm in streets and combined residential and industrial (resind) areas, as well as total inundation for the reference scenario. The relative difference in inundation of four different blockage scenarios is listed as comparison. These blockage scenarios share the same blockage ratios $BR = 0.8$ and trigger ratios $TR = 1.2$, except for the scenarios in which installed mitigation measures are simulated at the critical culverts 1 (cc1), 2 (cc2) or both (cc1,2) by applying $TR = \infty$.

		HN5	**HN10**	**HN20**	**HN30**	**HN50**	**HN100**
Reference, area with absolute inundation > 30 cm [m^2]	Street	2434	4266	8402	11726	17803	26299
	Resind	977	1495	2365	3468	5263	8248
	Total	57117	82445	112880	137398	178906	250673
BR=0.8, TR=1.2, relative diff. [%]	Street	18.49%	13.22%	13.32%	7.53%	4.54%	1.48%
	Resind	4.40%	1.87%	18.31%	13.87%	7.70%	0.42%
	Total	2.81%	1.75%	2.88%	2.54%	1.80%	0.86%
BR=0.8, TR=1.2, cc1 TR=∞, relative diff. [%]	Street	1.40%	8.77%	12.88%	6.90%	3.93%	1.26%
	Resind	0.10%	0.87%	18.18%	13.64%	7.37%	0.46%
	Total	1.74%	1.38%	2.77%	2.43%	1.72%	0.91%
BR=0.8, TR=1.2, cc2 TR=∞, relative diff. [%]	Street	18.37%	13.48%	1.37%	0.31%	2.45%	0.12%
	Resind	4.20%	1.74%	0.47%	0.32%	1.56%	-1.75%
	Total	2.68%	1.60%	1.29%	1.36%	1.50%	0.44%
BR=0.8, TR=1.2, cc1,2 TR=∞, relative diff. [%]	Street	1.19%	1.76%	1.31%	-0.03%	1.97%	-0.07%
	Resind	-0.10%	0.20%	0.46%	-0.20%	1.48%	-1.73%
	Total	1.62%	0.90%	1.31%	1.37%	1.43%	0.53%

https://doi.org/10.5194/egusphere-2025-5228
Preprint. Discussion started: 25 November 2025

Author contributions. All authors contributed to the concept and developed methods. LFDV and KM generated the models and managed data pre- and postprocessing. LFDV adapted the code for culverts in TELEMAC. LFDV was in charge of the main analysis and was responsible for writing the original draft for submission. KM and DCV also contributed to the generation of figures, writing and reviewing the figures.

Competing interests. The contact author has declared that none of the authors has any competing interests.

Data availability. The rastered maximum water depths can be openly retrieved at:
https://osf.io/6m5nb/?view_only=c3f6c563d4bc44ff844bfa48d2038116

Acknowledgements. We want to thank the German ministry for Education and Research for funding this study within the Inno_MAUS project. Furthermore, we thank Professor Axel Bronstert, Dr. Maik Heistermann, Dr. Guilherme Samprogna Mohor and Sarah Lindenlaub for supporting this study within the project. We thank Moritz Reininger for providing photographs of recent flood events in the catchment and the fire department of Reichenberg for their cooperation. Finally, we thank Florian Brunner and Burak Gür for assisting in the field study and Marko Kajo for testing setups of the blockage implementation in TELEMAC-2D. We also acknowledge the usage of Grammarly and Chat-GPT to locate grammatical errors in this paper.

https://doi.org/10.5194/egusphere-2025-5228
Preprint. Discussion started: 25 November 2025

References

Ah-Woane, E., Amama, Z., Cordier, F., Davarend, T., Lotfi, J., Assaba, M., Sochinskii, A., Majdalani, S., Moussa, R., Abily, M., and Delestre, O.: Toward Brague river flood modelling 3: the impact of culvert representation, Digital Water, 3, 1–22, https://doi.org/10.1080/28375807.2025.2465376, 2025.

Apel, H., Aronica, G., Kreibich, H., and Thieken, A.: Flood risk analyses-how detailed do we need to be? Nat Hazard, Natural Hazards, 49, 79–98, https://doi.org/10.1007/s11069-008-9277-8, 2008.

Archer, D., O'Donnell, G., Lamb, R., Warren, S., and Fowler, H. J.: Historical flash floods in England: New regional chronologies and database, Journal of Flood Risk Management, 12, e12 526, https://doi.org/https://doi.org/10.1111/jfr3.12526, 2019.

Ball, J., Babister, M., Nathan, R., Weeks, W., Weinmann, E., Retallick, M., and Testoni, I.: Australian Rainfall and Runoff: A Guide to Flood Estimation, Commonwealth of Australia (Geoscience Australia), ISBN 978-1-925848-36-6, 2019.

Bartels, H., Weigl, E., Reich, T., Lang, P., Wagner, A., Kohler, O., and Gerlach, N.: Projekt RADOLAN-Routineverfahren zur Online-Aneichung der Radarniederschlagsdaten mit Hilfe von automatischen Bodenniederschlagsstationen (Ombrometer): zusammenfassender Abschlussbericht für die Projektlaufzeit von 1997 bis 2004, Tech. rep., Deutscher Wetterdienst (DWD), 2004.

Bayerisches Landesamt für Umwelt, ed.: Klima-Faktenblätter Bayern und Mainregion – Klima der Vergangenheit und Zukunft, Bayerisches Landesamt für Umwelt, Augsburg, Germany, 2021.

Bayón, A., Valero, D., and Franca, M. J.: Urban flood drifters (UFD): Identification, classification and characterisation, Journal of Flood Risk Management, 17, https://doi.org/10.1111/jfr3.13002, 2024.

Bodhaine, G. L.: Measurement of peak discharge at culverts by indirect methods, US Government Printing Office Washington, DC, 1968.

Borga, M., Gaume, E., Creutin, J., and Marchi, L.: Surveying flash floods: Gauging the ungauged extremes, Hydrological Processes - HYDROL PROCESS, 22, 3883–3885, https://doi.org/10.1002/hyp.7111, 2008.

Borga, M., Stoffel, M., Marchi, L., Marra, F., and Jakob, M.: Hydrogeomorphic response to extreme rainfall in headwater systems: Flash floods and debris flows, Journal of Hydrology, 518, 194–205, https://doi.org/https://doi.org/10.1016/j.jhydrol.2014.05.022, climatic change impact on water: Overcoming data and science gaps, 2014.

Bowling, L. C. and Lettenmaier, D. P.: Evaluation of the effects of forest roads on streamflow in Hard and Ware Creeks, Tech. rep., University of Washington, 1997.

Burghardt, L., Klopries, E.-M., and Schüttrumpf, H.: Structural damage, clogging, collapsing: Analysis of the bridge damage at the rivers Ahr , Inde and Vicht caused by the flood of 2021, Journal of Flood Risk Management, 18, https://doi.org/10.1111/jfr3.13001, 2025.

Caretta, M., Mukherji, A., Arfanuzzaman, Betts, R., Gelfan, A., Hirabayashi, Y., Lissner, T., Liu, J., Lopez Gunn, E., Morgan, R., Mwanga, S., and Supratid, S.: Water, in: Climate Change 2022: Impacts, Adaptation and Vulnerability. Contribution of Working Group II to the Sixth Assessment Report of the Intergovernmental Panel on Climate Change, edited by Pörtner, H.-O., Roberts, D., Tignor, M., Poloczanska, E., Mintenbeck, K., Alegría, A., Craig, M., Langsdorf, S., Löschke, S., Möller, V., Okem, A., and Rama, B., pp. 551–712, Cambridge University Press, Cambridge, UK and New York, NY, USA, https://doi.org/10.1017/9781009325844.006, 2022.

Caviedes-Voullième, D., García-Navarro, P., and Murillo, J.: Influence of mesh structure on 2D full shallow water equations and SCS Curve Number simulation of rainfall/runoff events, Journal of Hydrology, 448-449, 39–59, https://doi.org/https://doi.org/10.1016/j.jhydrol.2012.04.006, 2012.

Collier, C. G.: Flash flood forecasting: What are the limits of predictability?, Quarterly Journal of the Royal Meteorological Society, 133, 3–23, https://doi.org/10.1002/qj.29, 2007.

https://doi.org/10.5194/egusphere-2025-5228
Preprint. Discussion started: 25 November 2025

De Vos, F., Wirthensohn, M., Broich, K., and Rüther, N.: Revised Implementation of the Green-Ampt Infiltration Method in TELEMAC-2D, in: Proceedings of 30th TELEMAC User Conference, 2024.

Deutsche Vereinigung für Wasserwirtschaft, Abwasser und Abfall: Arbeitsblatt DWA-A 118: Hydraulische Bemessung und Nachweis von Entwässerungssystemen, Deutsche Vereinigung für Wasserwirtschaft, Abwasser und Abfall, Hennef, ISBN 978-3-887-21924-6, 2006.

DWD Climate Data Center (CDC): Recent hourly RADOLAN grids of precipitation depth (GIS-readable), version 2.5, 2025.

EDF: TELEMAC-2D: User Manual. Version v8p4, EDF, 2022.

Erpicum, S., Poppema, D., Burghardt, L., Benet, L., Wüthrich, D., Klopries, E.-M., and Dewals, B.: A dataset of floating debris accumulation at bridges after July 2021 flood in Germany and Belgium, Scientific data, 11, 1092, https://doi.org/10.1038/s41597-024-03907-8, 2024.

Esri: "Satellite" [basemap]. Scale Not Given. "World Imagery", https://www.arcgis.com/home/item.html?id=10df2279f9684e4a9f6a7f08febac2a9, 2025.

Fernández-Pato, J., Martínez-Aranda, S., Morales-Hernández, M., and García-Navarro, P.: Analysis of the performance of different culvert boundary conditions in 2D shallow flow models, Journal of Hydroinformatics, 22, 1093–1121, https://doi.org/10.2166/hydro.2020.025, 2020.

Feuerwehr Reichenberg: Flood Protection Operation July 15th, 2021, https://ff-reichenberg.de/einsatzberichte/1775-hochwasser-keller-unter-wasser/, accessed: (24.04.2025), 2021a.

Feuerwehr Reichenberg: Flood Protection Operation July 9th, 2021, https://ff-reichenberg.de/einsatzberichte/1752-hochwasser-strasse-ueberflutet/, accessed: (24.04.2025), 2021b.

Feuerwehr Reichenberg: Fire Department Operations in 2021, https://ff-reichenberg.de/einsatzberichte/2021/, accessed: (24.04.2025), 2021c.

Feuerwehr Reichenberg: Flood Protection Operation August 3rd, 2024, https://ff-reichenberg.de/einsatzberichte/4944-hochwasser-strasse-uebeflutet/, accessed: (24.04.2025), 2024.

Gaume, E., Bain, V., Bernardara, P., Newinger, O., Barbuc, M., Bateman, A., Blaškovičová, L., Blöschl, G., Borga, M., Dumitrescu, A., Daliakopoulos, I., Garcia, J., Irimescu, A., Kohnova, S., Koutroulis, A., Marchi, L., Matreata, S., Medina, V., Preciso, E., Sempere-Torres, D., Stancalie, G., Szolgay, J., Tsanis, I., Velasco, D., and Viglione, A.: A compilation of data on European flash floods, Journal of Hydrology, 367, 70–78, https://doi.org/https://doi.org/10.1016/j.jhydrol.2008.12.028, 2009.

Georgakakos, K.: Real-Time Flash Flood Prediction, Journal of Geophysical Research, 92, 9615–9629, https://doi.org/10.1029/JD092iD08p09615, 1987.

Green, W. H. and Ampt, G. A.: Studies on Soil Physics, The Journal of Agricultural Science, 4, 1–24, https://doi.org/10.1017/S0021859600001441, 1911.

Hawkins, R. H.: Runoff curve numbers with varying site moisture, Journal of the irrigation and drainage division, 104, 389–398, 1978.

Iqbal, U. and Riaz, M. Z. B.: Blockage at cross-drainage hydraulic structures - Advances, challenges and opportunities, Heliyon, 10, e35 786, https://doi.org/10.1016/j.heliyon.2024.e35786, 2024.

Junghänel, T., Bär, F., Deutschländer, T., Haberlandt, U., Otte, I., Shehu, B., Stockel, H., Stricker, K., Thiele, L., and Willems, W.: Methodische Untersuchungen zur Novellierung der Starkregenstatistik für Deutschland (MUNSTAR), Tech. rep., Tech. rep., Synthesebericht, 2022.

Khosh Bin Ghomash, S., Apel, H., and Caviedes-Voullième, D.: Are 2D shallow-water solvers fast enough for early flood warning? A comparative assessment on the 2021 Ahr valley flood event, Natural Hazards and Earth System Sciences, 24, 2857–2874, https://doi.org/10.5194/nhess-24-2857-2024, 2024.

https://doi.org/10.5194/egusphere-2025-5228
Preprint. Discussion started: 25 November 2025

Khosh Bin Gomash, S., Deng, S., Spazier, J., and Apel, H.: Enabling Real-Time High-Resolution Flood Forecasting for the Entire State of Berlin Through RIM2D's Multi-GPU Processing, EGUsphere [preprint], https://doi.org/10.5194/egusphere-2025-2425, 2025.

Li, C., Jiang, C., Chen, J., Lam, M. Y., Xia, J., and Ahmadian, R.: An overview of flood evacuation planning: Models, methods, and future directions, Journal of Hydrology, 656, 133 026, https://doi.org/https://doi.org/10.1016/j.jhydrol.2025.133026, 2025.

Ligier, P. L.: Implementation of a rainfall-runoff model in TELEMAC-2D, in: Proceedings of XXIIIrd TELEMAC-MASCARET User Conference, 2016.

Lo´czy, D., Cziga´ny, S., and Pirkhoffer, E.: Flash Flood Hazards, in: Studies on Water Management Issues, edited by Kumarasamy, M., chap. 2, IntechOpen, Rijeka, https://doi.org/10.5772/28775, 2012.

LUBW: Kommunales Starkregenrisikomanagement in Baden-Württemberg, LUBW, 2020.

Miranzadeh, A., Keshavarzi, A., and Hamidifar, H.: Blockage of box-shaped and circular culverts under flood event conditions: a laboratory investigation, International Journal of River Basin Management, 21, 607–616, https://doi.org/10.1080/15715124.2022.2064483, 2023.

Molinari, D., Scorzini, A. R., Arrighi, C., Carisi, F., Castelli, F., Domeneghetti, A., Gallazzi, A., Galliani, M., Grelot, F., Kellermann, P., Kreibich, H., Mohor, G. S., Mosimann, M., Natho, S., Richert, C., Schroeter, K., Thieken, A. H., Zischg, A. P., and Ballio, F.: Are flood damage models converging to "reality"? Lessons learnt from a blind test, Natural Hazards and Earth System Sciences, 20, 2997–3017, https://doi.org/10.5194/nhess-20-2997-2020, 2020.

Okamoto, T., Takebayashi, H., Sanjou, M., Suzuki, R., and Toda, K.: Log jam formation at bridges and the effect on floodplain flow: A flume experiment, Journal of Flood Risk Management, 13, https://doi.org/10.1111/jfr3.12562, 2019.

Ollett, P., Syme, B., and Ryan, P.: Australian Rainfall and Runoff guidance on blockage of hydraulic structures: numerical implementation and three case studies, Journal of Hydrology (New Zealand), 56, 109–122, 2017.

Pizzileo, S., Moretti, G., and Orlandini, S.: Flood plain inundation modeling with explicit description of land surface macrostructures, Advances in Water Resources, 188, 104 713, https://doi.org/https://doi.org/10.1016/j.advwatres.2024.104713, 2024.

Reinert, J., Dittmer, C., Lorenz, D., and Klopries, E.-M.: Design Flaws at the Interface of Flood Forecasting, Early Warning and Disaster Response in the Disaster in Western Germany in July 2021—An Interdisciplinary Analysis, Journal of Flood Risk Management, 18, 70 099, https://doi.org/10.1111/jfr3.70099, 2025.

Rigby, E. and Barthelmess, A.: Culvert Blockage Mechanisms and their Impact on Flood Behaviour, in: Proceedings of the 34th IAHR world congress, 2011.

Rigby, E., Boyd, M., Roso, S., Silveri, P., and Davis, A.: Causes and Effects of Culvert Blockage During Large Storms, Ninth International Conference on Urban Drainage, https://doi.org/10.1061/40644(2002)298, 2002.

Robinson, A., Lehmann, J., Barriopedro, D., Rahmstorf, S., and Coumou, D.: Increasing heat and rainfall extremes now far outside the historical climate, npj Climate and Atmospheric Science, 4, 45, https://doi.org/10.1038/s41612-021-00202-w, 2021.

Rohmat, F. I. W., Sa'adi, Z., Stamataki, I., Kuntoro, A. A., Farid, M., and Suwarman, R.: Flood modeling and baseline study in urban and high population environment: A case study of Majalaya, Indonesia, Urban Climate, 46, 101 332, https://doi.org/https://doi.org/10.1016/j.uclim.2022.101332, 2022.

Schubert, J. E. and Sanders, B. F.: Building treatments for urban flood inundation models and implications for predictive skill and modeling efficiency, Advances in Water Resources, 41, 49–64, https://doi.org/https://doi.org/10.1016/j.advwatres.2012.02.012, 2012.

Sellevold, J., Norem, H., Bruland, O., Rüther, N., and Pummer, E.: Effects of Bottom-Up Blockage on Entrance Loss Coefficients and Head-Discharge Relationships for Pipe Culvert Inlets: Comparisons of Theoretical Methods and Experimental Results, Journal of Irrigation and Drainage Engineering, 150, https://doi.org/10.1061/JIDEDH.IRENG-10219, 2024.

https://doi.org/10.5194/egusphere-2025-5228
Preprint. Discussion started: 25 November 2025

Shewchuk, J. R.: Triangle: Engineering a 2D Quality Mesh Generator and Delaunay Triangulator, in: Applied Computational Geometry: Towards Geometric Engineering, edited by Lin, M. C. and Manocha, D., vol. 1148 of *Lecture Notes in Computer Science*, pp. 203–222, Springer-Verlag, from the First ACM Workshop on Applied Computational Geometry, 1996.

Smolders, S. and Bourbain, S.: Applications of the new simplified approach to model obstacles: weirs, culverts and virtual ponds, Proceedings of the 30th TELEMAC User Conference, 2024.

Smolders, S., Leroy, A., Teles, M. J., Maximova, T., and Vanlede, J.: Culverts modelling in TELEMAC-2D and TELEMAC-3D, Proceedings of the 23rd TELEMAC User Conference, pp. 21–33, 2016.

U.S. Department of Agriculture, Soil Conservation Service: National Engineering Handbook, Section 4: Hydrology, Chapter 10: Estimation of Direct Runoff from Storm Rainfall, U.S. Department of Agriculture, Washington, D.C., nEH Notice 4-102, August 1972, 1972.

Valero, D., Bayón, A., and Franca, M. J.: Urban Flood Drifters (UFDs): Onset of movement, The Science of the total environment, 927, 171 568, https://doi.org/10.1016/j.scitotenv.2024.171568, 2024.

Voit, P. and Heistermann, M.: A downward-counterfactual analysis of flash floods in Germany, Natural Hazards and Earth System Sciences, 24, 2147–2164, https://doi.org/10.5194/nhess-24-2147-2024, 2024.

Weeks, B., Barthelmess, A., Rigby, E., Witheridge, G., and O'Loughlin, G.: Project 11: Blockage of Hydraulic Structures. Stage 1 Report, Engineers Australia, 2013.

Wing, O. E. J., Pinter, N., Bates, P. D., and Kousky, C.: New insights into US flood vulnerability revealed from flood insurance big data, Nature Communications, 11, 1444, https://doi.org/10.1038/s41467-020-15264-2, 2020.

Winterrath, T., Brendel, C., Hafer, M., Junghänel, T., Klameth, A., Lengfeld, K., Walawender, E., Weigl, E., and Becker, A.: Radar climatology (RADKLIM) version 2017.002; gridded precipitation data for Germany, https://doi.org/10.5676/DWD/RADKLIM _YW_V2017.002, 2018a.

Winterrath, T., Brendel, C., Hafer, M., Junghänel, T., Klameth, A., Lengfeld, K., Walawender, E., Weigl, E., and Becker, A.: Radar climatology (RADKLIM) version 2017.002; gridded precipitation data for Germany, https://doi.org/10.5676/DWD/RADKLIM_RW_V2017.002, 2018b.